SUBTASK 2.6 – OPTIMIZATION OF AEROSOL MITIGATION TECHNOLOGY FOR POSTCOMBUSTION CO_2 CAPTURE

Topical Report

(for the period of September 1, 2019, through February 28, 2021)

Prepared for:

AAD Document Control

National Energy Technology Laboratory
U.S. Department of Energy
626 Cochrans Mill Road
PO Box 10940, MS 921-107
Pittsburgh, PA 15236-0940

Cooperative Agreement No.: DE-FE0024233
DOE Technical Monitor: Isaac A. Aurelio

Prepared by:

Jason D. Laumb
Joshua R. Strege
John P. Kay
Joshua J. Stanislowski

Energy & Environmental Research Center
University of North Dakota
15 North 23rd Street, Stop 9018
Grand Forks, ND 58202-9018

2021-EERC-02-05 February 2021

EERC DISCLAIMER

LEGAL NOTICE This research report was prepared by the Energy & Environmental Research Center (EERC), an agency of the University of North Dakota, as an account of work sponsored by the U.S. Department of Energy National Energy Technology Laboratory. Because of the research nature of the work performed, neither the EERC nor any of its employees makes any warranty, express or implied, or assumes any legal liability or responsibility for the accuracy, completeness, or usefulness of any information, apparatus, product, or process disclosed or represents that its use would not infringe privately owned rights. Reference herein to any specific commercial product, process, or service by trade name, trademark, manufacturer, or otherwise does not necessarily constitute or imply its endorsement or recommendation by the EERC.

ACKNOWLEDGMENT

This material is based upon work supported by the U.S. Department of Energy, National Energy Technology Laboratory under Award No. DE-FE-0024233.

DOE DISCLAIMER

This report was prepared as an account of work sponsored by an agency of the United States Government. Neither the United States Government, nor any agency thereof, nor any of their employees, makes any warranty, express or implied, or assumes any legal liability or responsibility for the accuracy, completeness, or usefulness of any information, apparatus, product, or process disclosed, or represents that its use would not infringe privately owned rights. Reference herein to any specific commercial product, process, or service by trade name, trademark, manufacturer, or otherwise does not necessarily constitute or imply its endorsement, recommendation, or favoring by the United States Government or any agency thereof. The views and opinions of authors expressed herein do not necessarily state or reflect those of the United States Government or any agency thereof.

TABLE OF CONTENTS

LIST OF FIGURES ii

LIST OF TABLES iv

ABBREVIATIONS AND ACRONYMS v

EXECUTIVE SUMMARY vii

INTRODUCTION AND BACKGROUND 1

GOALS AND OBJECTIVES 4

PROJECT STRUCTURE AND RESEARCH METHODS 4

AEROSOL CHARACTERIZATION 5
- Initial Pilot-Scale Evaluations 5
  - Initial Parametric Slipstream Testing at MRY2 8
  - Dekati Stage Impactor Sampling 13
  - WESP Specifications 18
- Second-Phase Pilot-Scale Evaluations 18
  - WESP Installation and Testing 18
  - Aerosol-Sampling Results 19
  - Parametric Aerosol Testing 22
  - WESP Impacts on Aerosol and Sulfur Speciation 25
  - Dekati Sampling 27
  - Dekati Substrate Analysis 27
- Solvent Analysis 29

CONCLUSIONS 34

MILESTONES 35

REFERENCES 36

PARTICULATE TEST DATA FROM RENTED WESP ..... Appendix A

LIST OF FIGURES

1 Amine emissions as a function of the number of soot particles and MEA emissions as a function of the amount of sulfuric acid aerosol particles 2

2 SONICKLEEN WESP with scaffolding 6

3 Flue gas supply pipe and return flexible duct 7

4 Inlet and exhaust pipes, sample ports, and purge air piping 8

5 Total aerosol concentration from NanoScan for Tests 1–5 11

6 Test 6 total aerosol concentration 12

7 Dekati staged impactor inlet PSD 14

8 Aerosol chemistries obtained from SEM analysis 15

9 WESP inlet particle morphology from Dekati Stage 11 16

10 WESP inlet aerosol morphology from Dekati Stage 9 16

11 WESP outlet aerosol morphology for Stage 9 17

12 WESP outlet aerosol morphology for Stage 8 17

13 Bulk chemistry of WESP inlet and outlet substrates determined by ICP–MS 18

14 Overall size distribution and concentration as measured by the SMPS 19

15 Overall calculated efficiency of the WESP 20

16 Calculated efficiency for the particle range of 100–200 nm 20

17 FTIR data at the inlet and outlet of the WESP 21

18 Total particulate at the scrubber inlet, WESP inlet, and WESP outlet during June 25 sampling 21

19 Schematic showing the gas path through the pilot test system 22

20 Particulate loading at the WESP outlet with SO_2 scrubber online 25

Continued . . .

LIST OF FIGURES (continued)

21 Total particulate loading at the WESP outlet with SO_2 scrubber off-line 25

22 Total particulate count by hour of day without the WESP 26

23 PSDs at WESP inlet as determined by Dekati measurements 27

24 Mean elemental chemical analysis of the particulate collected on Stage 7 of the Dekati ... 28

25 Metal concentrations in solutions of digested Dekati substrates 28

26 WESP inlet morphology from Stages 7 and 15 29

27 Concentrations of major cations in the solvent..... 31

28 Concentrations of trace elements (Pb, Co, V, Hg, Cr, Ni, Mn, Se) in the solvent..... 32

29 Concentrations of trace elements (Fe, Cu, Zn, Al) in the solvent..... 33

30 Concentrations of anions and HSS in the solvent..... 34

LIST OF TABLES

1 Design and Operating Data for SONICKLEEN WESP 5

2 Completed WESP and Aerosol Sampling Test Conditions 9

3 Aerosol Measurement Instruments 9

4 Staged Impactor Sampling Periods and Aerosol Mass Concentrations 14

5 Staged Impactor Average Aerosol Mass Concentration 14

6 Total Aerosol Particle Counts Measured at the Inlet and Outlet of the WESP 20

7 Test Matrix for FTIR Sampling at the WESP Outlet 23

8 Test Matrix for FTIR Sampling at the Absorber Outlet 23

9 Test Matrix for Aerosol Sampling at the WESP Outlet 24

10 Test Matrix for Aerosol Sampling at Absorber Outlet 24

11 Solvent Constituents Analyzed by ICP/ICP–MS 30

12 Milestones 35

ABBREVIATIONS AND ACRONYMS

°F	degrees Fahrenheit
µm	micrometer
acfm	actual cubic foot per minute
$CaSO_3$	calcium sulfite
CCS	carbon capture and storage
cm^3	centimeter, cubed
CO	carbon monoxide
CO_2	carbon dioxide
CPVC	chlorinated polyvinyl chloride
DCC	direct contact cooler
DOE	U.S. Department of Energy
EERC	Energy & Environmental Research Center
ELPI	electrical low-pressure impactor
EOR	enhanced oil recovery
ESP	electrostatic precipitator
FGD	flue gas desulfurization [unit]
FESEM	field emission scanning electron microscope
ft	feet
FTIR	Fourier transform infrared [spectroscopy]
H_2O	water
H_2SO^4	sulfuric acid
HEPA	high-efficiency particulate air
hr	hour
HSS	heat-stable salts
ICP	inductively coupled plasma
ICP–MS	inductively coupled plasma–mass spectrometer
ID	induced draft
kV	kilovolt
kW	kilowatt
lb	pound
m^3	cubic meter
mA	milliamp
MDEA	methyldiethanolamine
MEA	monoethanolamine
mg	milligram
mg/Nm^3	milligram per normal meter, cubed
mL	milliliter
MPC	Minnkota Power Cooperative
MRY	Milton R. Young Station
MRY2	Milton R. Young Station Unit 2
NDIC	North Dakota Industrial Commission

continued . . .

ABREVIATIONS AND ACRONYMS (continued)

NETL	National Energy Technology Laboratory
nm	nanometer
NO_x	nitrogen oxides
PCCC	postcombustion carbon capture
PIP	piperazine
ppb	parts per billion
ppm	parts per million
PSD	particle-size distribution
scfm	standard cubic foot per minute
SEM	scanning electron microscopy
SMPS	scanning mobility particle sizer
SO_x	sulfur oxides
SO_2	sulfur dioxide
SO_3	sulfur trioxide
TIC	total inorganic carbon
WESP	wet electrostatic precipitator

SUBTASK 2.6 – OPTIMIZATION OF AEROSOL MITIGATION TECHNOLOGY FOR POSTCOMBUSTION CO_2 CAPTURE

EXECUTIVE SUMMARY

Growing concerns over the impact of CO_2 emissions from combustion sources on global climate change have prompted numerous research and development projects aimed at developing cost-effective technologies for CO_2 capture. One family of technologies being demonstrated at pilot and full scale globally is postcombustion CO_2 capture (PCCC) systems that employ amine-based solvents. The captured CO_2 can be compressed and permanently stored underground or used for enhanced oil recovery (EOR). The proximity of North Dakota's lignite-fired fleet of power plants to potential CO_2 storage options creates a unique atmosphere for PCCC within the state. However, the aerosols present in lignite flue gas present a challenge for large-scale PCCC at North Dakota power plants.

Aerosols can negatively impact the long-term performance of amine-based solvents for CO_2 capture. Amine-based solvents are volatile, and aerosols provide nucleation sites where amine vapors can condense. Because aerosols cannot be easily captured at the column outlet using conventional technologies, the amine-laden aerosols escape the system and lead to accelerated solvent losses. Moreover, aerosol components can chemically react with amines to form degradation products that can permanently deactivate the amine, cause fouling, and lead to hazardous emissions.

Many of the elements that have been shown to catalyze solvent degradation are present in lignite coals and can exacerbate solvent replacement economics. Understanding this issue is critical to the implementation of solvent-based CO_2 capture systems as applied to lignite-fired generation systems.

The Energy & Environmental Research Center (EERC) designed and carried out this project to optimize aerosol mitigation technology for PCCC at a lignite-fired power plant. To meet the goal of this project, the following objectives were identified:

- Determine the effectiveness of a wet electrostatic precipitator (WESP) on collection of aerosols at a low-rank coal-fired power station.

- Determine the impact of aerosols on the efficiency and degradation products of amine-based carbon capture systems fired with low-rank fuels.

Work was conducted at Minnkota Power Cooperative's (MPC's) Milton R. Young (MRY) Station Unit 2 using a slipstream of flue gas from the outlet of the plant's flue gas desulfurization (FGD) unit. To gather initial data for sizing and specifying a WESP for this system, a temporary pilot-scale WESP was rented and installed on-site. Several different conditions were tested to examine the impact of flow rate, voltage, and current on WESP performance. The WESP was effective at removing large particulate (>200 nm) but caused an increase in fine particulate (<75 nm). Fine particulate material at the inlet and outlet of the WESP was collected, analyzed, and showed that crystalline sulfates carried over from the plant's FGD unit were being converted to fine aerosols and SO_2 was being converted to SO_3 through the WESP. Additionally, the high

moisture content of the flue gas stream at this sample location also contributed to an overall increase in aerosol mass under some of the test conditions.

Using the results from the rented WESP, the project team installed a smaller-scale WESP upstream of the EERC's slipstream CO_2 capture system. Flue gas was routed through a pilot-scale FGD unit to remove SO_2 to very low levels (~1 ppm) and then through a direct contact cooler (DCC) to further cool the gas and to remove moisture. The gas exiting the DCC was then routed through the new WESP before passing to the CO_2 absorber columns. Fluor's amine-based solvent was used to scrub CO_2 from the slipstream through a set of two absorber columns. The rich solvent was regenerated in a stripper column by heating to drive off captured CO_2. The system operated using a catch-and-release method where the CO_2 was separated to provide data on the process, but the captured CO_2 was released back into the host site stack.

Aerosols and sulfur species were measured at multiple locations throughout the pilot-scale system. The inlet FGD and DCC removed much of the particulate matter and gaseous sulfur upstream of the WESP. With this configuration, the WESP achieved >95% particulate capture. The new WESP did not show any of the increases in SO_3 or other aerosol species that had been consistently observed with the larger-scale WESP installed immediately downstream of the plant's full-scale FGD unit. Particulate samples captured and analyzed from the WESP inlet did not show any presence of crystalline sulfate materials, indicating that the pilot-scale FGD and DCC were efficient at reducing carryover from the plant's full-scale FGD unit.

A set of parametric tests were conducted on the new WESP to assess the impacts of flow rate, voltage, number of online WESP fields, and gas-phase sulfur content on aerosol and sulfur transformations. The results showed that the WESP performed similarly well at all sets of conditions.

Sulfur and particulate matter exiting the WESP were further reduced through the absorber column as the amine-based solvent captured some of the residual contaminants. Solvent analysis showed that these species were slowly concentrating in the solvent over the duration of the test. When the WESP was taken offline and the sulfur slip through the FGD allowed to rise, the sulfate content in the solvent rose sharply, showing that the extra FGD and WESP were effective at reducing sulfate and cation uptake. This would be expected to extend amine-based solvent life by slowing the formation of heat-stable salts and other degradation products.

This subtask was cofunded through the EERC–U.S. Department of Energy Joint Program on Research and Development for Fossil Energy-Related Resources Cooperative Agreement No. DE-FE0024233. Nonfederal funding was provided by the North Dakota Industrial Commission and MPC.

SUBTASK 2.6 – OPTIMIZATION OF AEROSOL MITIGATION TECHNOLOGY FOR POSTCOMBUSTION CO_2 CAPTURE

INTRODUCTION AND BACKGROUND

With respect to societal desires to reduce carbon emissions, the long-term continued use of coal or any fossil fuel will likely depend on reducing its carbon intensity. CCS (carbon capture and storage) appears to be the most feasible option open to utilities to achieve such reductions, and North Dakota is fortunate to have proximal, large-scale sequestration potential in the form of enhanced oil recovery (EOR) in the state's conventional oil fields and in the Bakken shale play (Agalliu et al., 2016). However, even with these advantages, establishing a market where coal-powered utilities provide CO_2 to oil producers is still dependent on a cost-effective method for CO_2 capture. In addition to the cost of capture, other challenges are present in market growth, advanced solvents, and the formation of aerosols. Aerosols can negatively impact postcombustion capture systems by degrading solvent and exacerbating solvent carryover. The purpose of this Energy & Environmental Research Center (EERC) project was to optimize aerosol mitigation strategies for postcombustion capture solvents to provide insights for commercial best practices for minimizing aerosols.

Reactive solvent-based scrubbers such as those using amine-based solvents, including monoethanolamine (MEA), methyldiethanolamine (MDEA), piperazine (PIP), and various blends are a leading method to control CO_2 emissions from coal-fired plants (Dutcher et al., 2015; Le Moullec et al., 2014; Luis, 2016; Wu et al., 2014). During an amine-based postcombustion CO_2 capture (PCCC) process, pretreated flue gas is contacted with aqueous amine solution in an absorber in a countercurrent fashion to remove CO_2. The CO_2-rich solution is then heated in a stripper/regenerator to release the captured CO_2, and the CO_2-lean solution is pumped back to the absorber for another cycle. Meanwhile, the treated flue gas is water-washed and discharged.

Most of the above-identified amines are volatile and, therefore, small amounts will be emitted to the atmosphere via the treated flue gas stream. Several studies (Brachert et al., 2014; Fulk, 2016; Kamijo et al., 2013; Khakharia, 2015; Mertens et al., 2014) have identified substantial levels of solvent emissions from amine-based CO_2 scrubbers. Aerosol-based emissions on the order of grams per Nm^3 have been reported, and these emissions are attributed to the presence of particles such as sulfuric acid aerosol droplets in the flue gas entering the scrubber. Aerosol-based solvent emission is emerging as a key challenge in the realization of a full-scale absorption–stripping-based PCCC plant.

The emission of solvent and its components can occur by means of i) vapor emissions due to the volatility, ii) carryover as a result of mechanical entrainment, and iii) aerosols. The first two means of emissions are well understood. Recently, aerosol-based emissions have been reported from typical PCCC pilot plants (Kamijo et al., 2013; Khakharia et al., 2013, 2014a; Mertens et al., 2013, 2014). These studies indicate that aerosol-based emissions can be significant, on the order of grams/Nm^3, as compared to mg/Nm^3 of vapor emissions. Moreover, they cannot be reduced by conventional countermeasures such as a water wash or a demister (Khakharia et al., 2014b).

Therefore, these emissions can lead to environmental hazard and huge solvent losses, increasing the operating cost (Khakharia, 2015).

Aerosol-based emission in a CO_2 capture absorber is a multiparameter phenomenon (Khakharia et al., 2015). In the above study, the three main parameters identified were i) the particle number concentration, ii) the supersaturation, and iii) the reactivity of the amine. The aerosol particles, in the range of 10^7–10^8/cm^3, were made up of H_2SO_4 and H_2O and generated by homogeneous nucleation of gas-phase SO_3 in a combustion flue gas. Although small, the aerosol droplets offer a surface for heterogeneous nucleation.

As shown in Figure 1, there is a clear correlation of MEA emissions with the change in inlet aerosol (soot and H_2SO_4) number concentration. MEA emission increases from 100 to 200 mg/Nm^3 as the soot number concentration increases from ~10^4 to 10^6/cm^3 and again doubles from about 600 to 1100 mg/Nm^3, while the H_2SO_4 particle number concentration increases by 1.6 times from ~10^8/cm^3. It must be noted that the absolute MEA emissions from this capture unit would not be the same as a large-scale capture facility because the exact MEA emissions strongly depend on many factors, including the presence of a direct contact cooler (DCC), water wash section, lean pH, and absorber temperature profile.

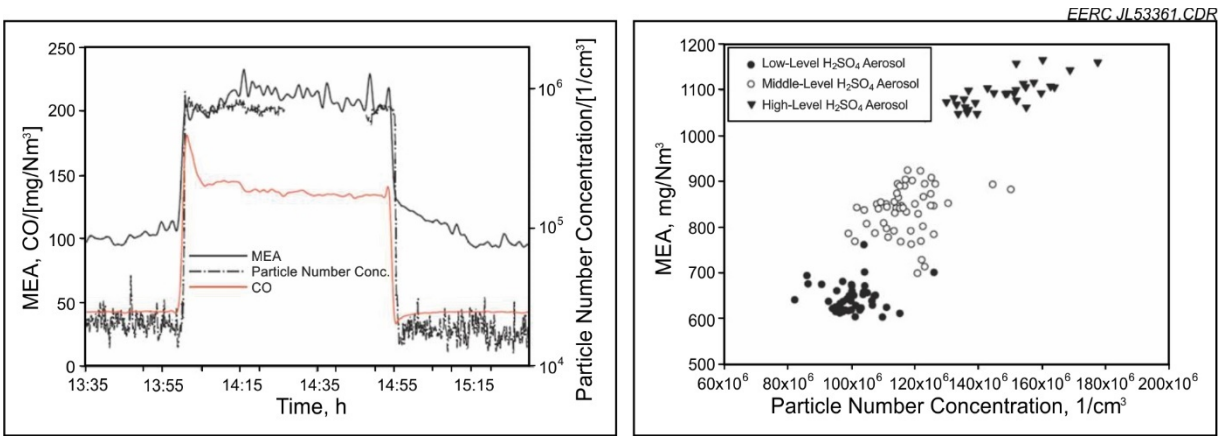

Figure 1. Amine emissions as a function of the number of soot (CO) particles (left) (Khakharia, 2015)and MEA emissions as a function of the amount of sulfuric acid aerosol particles (right) (Khakharia, 2015).

In an MEA solvent absorber, the flue gas heats as it rises through the column because the reaction of the solvent component with CO_2 generates heat. At the top of the column, the flue gas comes into contact with cold lean solvent, and the gas temperature rapidly drops as it approaches the absorber outlet. This leads to a so-called temperature bulge, where the temperature reaches a maximum, typically at a distance of two-thirds of the total packing height from the bottom. This can lead to a significant temperature difference between the gas and liquid phases, resulting in a supersaturated environment. Aerosols may act as nuclei where volatile components easily condense under supersaturation, leading to a growth of aerosol droplets. This form of aerosol-

based emission of MEA can be decreased by increasing the temperature of the lean solvent, but this leads to an increase in vapor emission.

Degradation of amines used to capture CO_2 from coal combustion flue gas impacts reliable operation because of corrosion and fouling but also increases operating costs and environmental issues (Chen et al., 2011; Fytianos et al., 2016; Kittel and Gonzalez, 2014; Veltman et al., 2010). The two main processes involved in the degradation of amines are thermal and oxidative. Excessively high temperatures cause thermal degradation, while oxidative degradation is due to the presence of oxygen, CO_2, and metal ions.

Extensive studies of degradation products of amines and the mechanism of their formation when exposed to coal combustion-derived flue gas have been conducted (Cuzuel et al., 2015; Gouedard et al., 2012, 2014; Rey et al., 2013). These papers discuss how the amines are degraded when they react with flue gas species that include O_2, CO_2, NO_x, SO_x, and others to produce degradation products. Some of the degradation products are toxic. The degradation research efforts have been aimed at understanding thermal degradation (carbamate polymerization), oxidative degradation, and formation of heat-stable salts (HSS). The most rapid process is oxidative degradation, because oxygen levels in the flue gas are typically 4% to 5% and the solvent is relatively reactive toward oxygen. Dissolved metals can catalyze the oxidative degradation process (Goff and Rochelle, 2004). Degradation of oxidized amines leads to the formation of HSS, and measurement of HSS is an indication of solvent degradation.

The accumulation of derived minor and trace elements in solvents exposed to coal combustion-derived flue gas has been examined by Schallert et al. (2013, 2014) and Nikolic et al. (2015). Nikolic et al. (2015) investigated the accumulation of arsenic, mercury, selenium, iron, nickel, and copper in selected amine-based solvents and found that the elements increase in concentration with time. They also noted that iron, nickel, and copper were found to accumulate less on one solvent as compared to the others tested, indicating that the type of solvent may impact the rate of accumulation. Therefore, solvent metal interactions need further study to determine the potential to accumulate as a function of aerosol particulate matter, consisting mainly of sodium, calcium, and sulfur (as sulfate) emitted from electrostatic precipitators (ESPs) and wet flue gas desulfurization (FGD) systems, when lignite is fired in a cyclone-fired boiler (Laumb et al., 2009). In addition, some potassium, iron, and other elements were also present in the aerosol samples examined. Based on work conducted by Schallert et al. (2013), ash particulate (aerosols) captured in the amine solvent can release elements such as iron, magnesium, and calcium into the solvent and are a concern for solvent degradation by the formation of HSS. The solubility of the elements in the solvent was dependent on the pH and CO_2 loading of the solvent. Schallert et al. (2013) also reported that in the stripper where the CO_2 level is reduced (increasing the pH), the solubility of the iron compounds was reduced, resulting in accumulation of deposits on stripper surfaces. Calcium was found to react with oxalate that also contributes to the formation of deposits on the reboiler, potentially causing the formation of deposits that can cause plugging and, possibly, corrosion. In a further study, Schallert et al. (2014) found that the degradation of amine solvent increased the mobility of manganese and vanadium.

This project—Subtask 2.6 under EERC–U.S. Department of Energy (DOE) Joint Program on Research and Development for Fossil Energy-Related Resources Cooperative Agreement No.

DE-FE0024233—was conducted to provide further insight into the effects of lignite-derived flue gas on amine-based PCCC solvents. Subtask 2.6 aimed to determine the impact of specific lignite-derived flue gas and ash components on degradation rates of a commercial solvent under several different gas treatment configurations. This study provided critical understanding on how gas treatment can help to mitigate the rate of solvent degradation to extend solvent life and to improve solvent replacement economics at a lignite-fired boiler.

Subtask 2.6 was performed over a period of 18 months, with a total budget of $1,125,000. The project was funded by DOE's National Energy Technology Laboratory (NETL) through the EERC's Cooperative Agreement, the North Dakota Industrial Commission (NDIC), and industry partner Minnkota Power Cooperative (MPC).

GOALS AND OBJECTIVES

The goal of Subtask 2.6 was to optimize aerosol mitigation technology for postcombustion CO_2 capture. In order to meet the goal of the project, the following objectives were identified:

- Determine the effectiveness of a wet ESP (WESP) on collection of aerosols at a low-rank coal-fired power station.
- Determine the impact of aerosols on the efficiency and degradation products of amine-based carbon capture systems fired with low-rank fuels.

PROJECT STRUCTURE AND RESEARCH METHODS

This project was roughly divided into two phases. During the first phase, a temporary WESP was rented and installed at Milton R. Young Station (MRY). A slipstream of flue gas from the Unit 2 stack was routed to the rented WESP, and several different operating conditions were studied to better understand the gas treatment requirements as well as the sizing and operating parameters needed to specify a more optimized WESP. This information was then used to specify and order a new WESP and to determine gas treatment configuration upstream of amine-based CO_2 capture column.

In the second phase of the project, a new WESP was ordered and installed in the gas treatment train of a small-scale amine-based CO_2 capture system. A slipstream of flue gas was routed to the system, with commercial Fluor solvent being used to capture CO_2 from the flue gas. The new WESP was tested under a variety of conditions to assess key parameters in achieving effective aerosol control to help extend solvent life.

Specific approaches taken during each of these phases are discussed in the sections that follow.

AEROSOL CHARACTERIZATION

Initial Pilot-Scale Evaluations

A key objective for the project was to test the effectiveness of a WESP at collecting fine particulate from a low-rank power station upstream of the absorber column to help reduce aerosol emissions at the column exit. To provide initial data needed to specify a custom-purpose WESP, the team rented a WESP to provide an assessment of fine particulate fate and likely operating conditions required for effective particulate control.

A pilot-scale SONICKLEEN WESP was rented from Durr-Megtec to provide initial data on WESP performance. This unit was capable of variable control of flow and corona voltage. The nominal design and operating data provided by Durr-Megtec are shown in Table 1. The system used a hexagonal vertical tube array with common walls between adjacent tubes, creating a honeycomb structure. Electrodes hung from an insulated high-voltage support grid. Heated purge air was used to keep the insulators clean. The purge air temperature was approximately 154°F.

Table 1. Design and Operating Data for SONICKLEEN WESP

Inlet Conditions		
Gas Flow (maximum – saturated)	acfm	2800
	scfm (dry)	1826
Temperature	°F	140
Pressure	inches w.c.	−25
Humidity	% v/v	20.6
Particulate Matter – Total	gr/dscf	0.0006
	lb/hr	0.010
Expected Outlet Conditions		
Gas Volume (with electrode purge air)	acfm	3534
Temperature	°F	140
Pressure	inches w.c.	−23.5
Humidity	% v/v	20.6
Particulate Matter – Total	gr/dscf	0.000191
	lb/hr	0.0038
Removal Efficiency	%	68.7
Design Parameters		
Pressure Drop Across WESP	inches W.C.	1.5
Gas Throughput Velocity	ft/sec	7.7
Effective Specific Collecting Area	SCA	129.9
SCA = ft^2/1000 acfm		
Electrical Power		
Precipitator–Transformer/Rectifiers	Quantity	1
Primary Power	V/Ph/Hz	460/3/60
Connected	kVA	11.16
Demand	kVA	2.01
Consumed	kW	1.45
Insulator Purge Heater	V/Ph/Hz	460/3/60
Connected	kVA	27
Consumed	kW	18.9

The SONICKLEEN WESP was installed on the ground rather than directly adjacent to the sampling point because of its size and weight. Scaffolding was installed around the unit to facilitate sampling activities. Figure 2 shows the WESP with scaffolding. The control room is located to the right of the WESP. The flush water holding tank and pump can be seen in the foreground. The large induced-draft (ID) fan used to draw flue gas through the WESP can be seen behind the water tank.

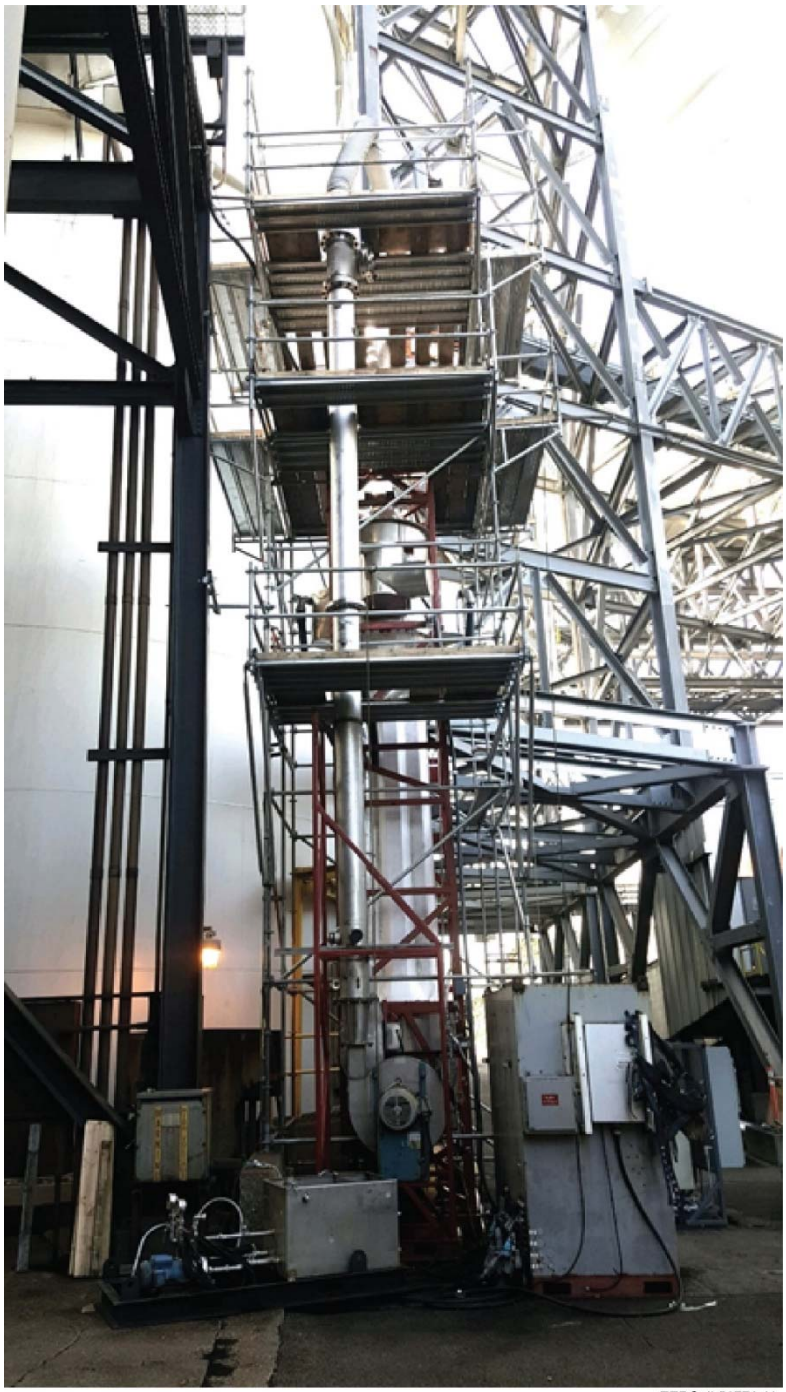

EERC JL56776.AI

Figure 2. SONICKLEEN WESP with scaffolding.

Flue gas supply and return ducting were installed to connect the WESP to the MRY Unit 2 (MRY2) flue gas duct at a point upstream of the entry to the stack. This location was representative of where a full-scale CO_2 capture system would be connected. The supply piping was 12"-diameter chlorinated polyvinyl chloride (CPVC) pipe, while the return was 12"-diameter spiral-wound flex duct, as shown in Figure 3.

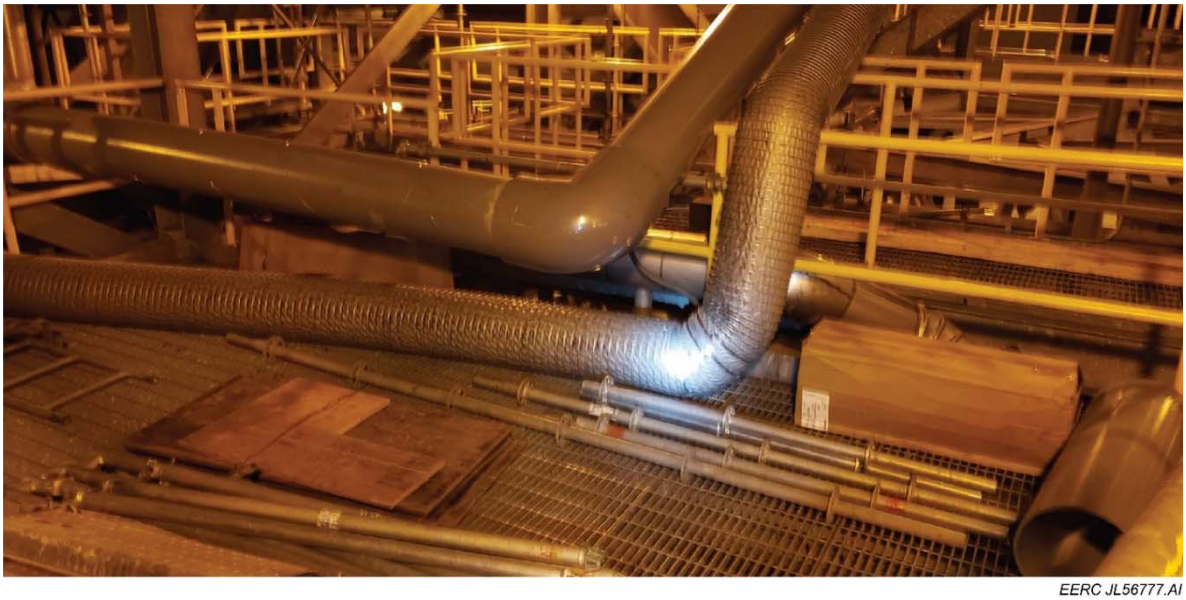

Figure 3. Flue gas supply pipe and return flexible duct.

Figure 4 shows the inlet and exhaust piping connected to the SONICKLEEN WESP and the locations of sample ports. The sample port locations were determined on the basis of access to the piping via scaffolding and straight laminar flow sections of pipe both upstream and downstream from the sample ports. The exhaust duct is directly above the ID fan. One of the three WESP insulator purge air piping units is also shown in Figure 4.

A parametric test matrix was developed to examine the effects of flow rates (residence time), corona voltages, and WESP current on particulate loading. Testing was conducted during the period of August 26–30, 2019.

Figure 4. Inlet and exhaust pipes, sample ports, and purge air piping.

Initial Parametric Slipstream Testing at MRY2

Table 2 shows the tests completed in August–September 2019 using the pilot-scale SONICKLEEN WESP unit rented from Durr–Megtec. Tests 1–5 were performed August 28 and 29. Tests 6–9 were performed September 4–6. The controllable variables for the tests were flue gas flow rate to the WESP and operating voltage/current. These variables were adjusted during the testing to determine the effect on aerosol and larger particulate removal.

Table 3 shows the instruments used to measure aerosol concentration and size distribution during the testing. These include a scanning mobility particle sizer (SMPS) from TSI, Incorporated; a portable NanoScan SMPS, also from TSI; and a Dekati 15-stage electrical low-pressure impactor (ELPI). The SMPS and NanoScan provided real-time data on particle-size distribution (PSD) and total particulate loading. The Dekati ELPI provided long-term collection of particulate matter on substrates that could then be recovered, weighed, and analyzed to assess

particulate mass distribution, structure, and chemical composition. For the SMPS and NanoScan, a dilution and drying assembly was used upstream of each device to condition the flue gas prior to measurement. The outlet location was especially challenging to measure given the saturated moisture content of the gas leaving the WESP. During testing, the inlet temperature was approximately 140°F, while the outlet temperature was 138°F.

Table 2. Completed WESP and Aerosol Sampling Test Conditions

Test No.	Date	Start Time	End Time	Flow Rate, acfm	Voltage, kV	Current, mA	NanoScan	SMPS
1	8/28	18:03	19:22	2700	60–75	40	Outlet	Inlet
2	8/29	10:31	11:59	2700	60–75	50	Outlet	Inlet
2	8/29	11:59	12:10	Ambient	Off	Off	Ambient	Inlet
2	8/29	12:10	12:24	2700	60–75	50	Outlet	Inlet
3	8/29	14:12	15:09	1800	60–75	44	Outlet	Inlet
3	8/29	15:35	16:24	1800	60–75	44	Inlet	Inlet
3	8/29	16:38	16:53	1800	60–75	44	Outlet	Inlet
4	8/29	18:03	18:23	1800	55–60	20	Outlet	Inlet
5	8/29	18:23	18:52	1800	60–75	38	Outlet	Inlet
6	9/4	9:53	11:38	1800	60–75	60	Outlet	Inlet
6	9/4	11:40	12:28	1800	Off	Off	Outlet	Inlet
6	9/4	12:30	17:02	Ambient	Off	Off	Ambient	Inlet
6	9/4	17:02	17:10	1800	60–75	60	Outlet	Inlet
7	9/4	17:10	17:26	1800	50	14	Outlet	Inlet
7	9/4	17:26	17:52	1800	Lowest – 40	9	Outlet	Inlet
8	9/5	11:02	11:45	2700	60–75	55	Outlet	Outlet
8	9/5	11:54	17:52	2700	60–75	55	Inlet	Outlet
9	9/6	8:29	11:09	2700	60–75	25	Inlet	Outlet
9	9/6	11:09	11:36	2700	60–75	25	Outlet	Outlet

Table 3. Aerosol Measurement Instruments

Instrument	Concentration	Size Range, nm
SMPS	$1–10^7$ (count/cm^3)	2.5–765
NanoScan SMPS	1–1,000,000 (count/cm^3)	10–420
Dekati Impactor	mg/Nm^3	16–10,000

The results are discussed by test number in the following sections. Figures showing aerosol concentrations and PSDs are included in Appendix A.

Test 1

Test 1 was performed at a flue gas flow rate of 2700 acfm, with WESP operating conditions of 60 to 75 kV and 40 mA. The inlet and outlet aerosol data (concentration and PSD) were measured by the SMPS and NanoScan, respectively.

The inlet particulate loading was found to be lower than the outlet on a total concentration basis, indicating that the WESP was generating rather than reducing fine particulate matter. Mass concentration at the outlet appeared to be similar to the mass loading at the inlet. The PSDs showed particulate reduction in the sizes over approximately 200 nm but an increase in aerosols in sizes smaller than 75 nm. The finding that the WESP generated fine aerosols was consistent throughout all the later tests.

Test 2

Test 2 repeated the Test 1 flow and voltage conditions. The particulate outlet concentration was higher than the inlet concentration in Test 2, as was observed in Test 1. Similarly, the PSD curve for Test 2 again clearly showed the particle-size shift through the WESP from larger particulate to smaller aerosols. Mass concentration comparison showed substantially higher particulate mass concentration at the outlet relative to the inlet. This increase was in contrast to the unchanged mass concentration observed during Test 1 and could be related to the high moisture content at the WESP outlet during this test.

Test 3

In Test 3, the flue gas flow to the WESP was 1800 acfm, compared to 2700 acfm for Tests 1 and 2. The WESP operating current was 44 mA, which was intermediate to values of 40 and 50 mA in Tests 1 and 2, respectively. There was no significant difference in the aerosol measurements in Test 3 at the lower flow rate relative to Tests 1 and 2. Large particulate was reduced, with very fine aerosol (<75 nm) generation occurring. The overall mass loading through the WESP was very low, single-digit mg/Nm^3.

To verify that the changes in particulate loading being measured through the WESP were not the result of differences in measuring devices, the NanoScan was briefly moved from the outlet to the inlet during this test. The NanoScan and was found to measure particulate concentration data very similarly to what the SMPS was measuring at the WESP inlet.

Test 4

Conditions for the short-duration (20-minute) Test 4 were a flue gas flow rate of 1800 acfm, a reduced voltage of 55–60 kV (relative to Tests 1–3), and a significantly reduced current of 20 mA. Test 4 results were similar to previous testing, with an appreciable reduction in large particulate accompanied by an increase in fine particulate.

Test 5

Test 5 was a repeat of Test 3 conditions, with the WESP operating at 1800 acfm and 60–75 kV. Again, the large particulate matter decreased while the <75-nm aerosol PSD concentration for the WESP outlet increased, this time by almost 2 orders of magnitude relative to the inlet concentration.

Tests 1–5 Comparison

Figure 5 shows the WESP total aerosol concentration, as measured by the NanoScan, during Tests 1–5. This plot suggests two results from operating the WESP and from varying flue gas flow rate and voltage/current. First, the WESP appeared to increase total particle concentration, as evidenced when the NanoScan measured the inlet aerosol concentration and when the WESP was inadvertently shut off while sampling was ongoing. Second, varying the flue gas flow rate and voltage/current did not affect outlet particle concentration.

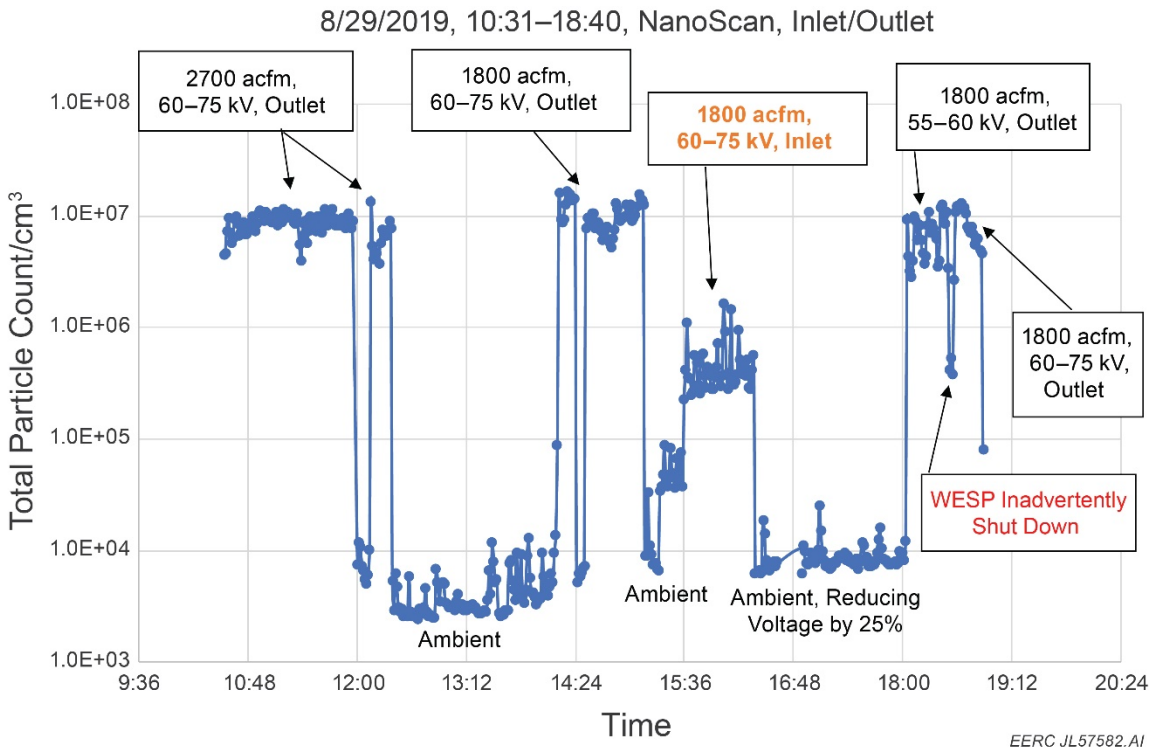

Figure 5. Total aerosol concentration from NanoScan for Tests 1–5.

Test 6

Building on observations from Tests 1–5, a series of parametric tests were performed during Test 6, with the NanoScan again measuring at the WESP outlet. Figure 6 presents the Test 6 total aerosol concentration, with notes included for critical changes in WESP operation or NanoScan

operation. The aerosol concentrations clearly increased when the WESP was turned on, with the WESP outlet concentration being almost 2 orders of magnitude higher than with the WESP off or when measuring inlet concentration.

Test 7

During Test 7, the WESP operating voltage was decreased to the lowest levels attainable, 40 to 50 kV, while the flue gas flow rate was maintained at 1800 acfm. Only NanoScan measurements at the outlet were obtained at this condition. The outlet PSD showed a very large peak of fine particulate matter and a total initial concentration similar to what was observed at the outlet in all other tests. The particulate loading dropped off halfway through Test 7 to levels similar to the WESP inlet, suggesting that the WESP may not have been affecting flue gas at this very low-voltage condition.

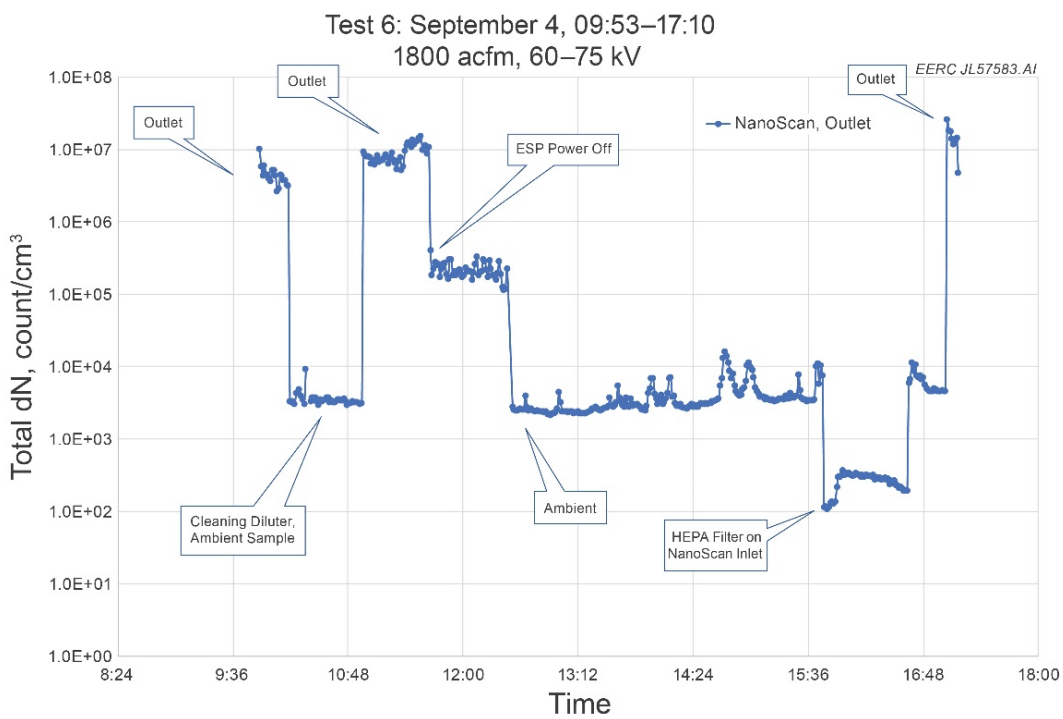

Figure 6. Test 6 total aerosol concentration (HEPA stands for high-efficiency particulate air).

Test 8

The flue gas flow rate was increased to 2700 acfm for Test 8. During the 6-hour (11:54 to 17:52) period of Test 8, the NanoScan and SMPS sampled at the WESP inlet and outlet, respectively. This was reversed from previous sampling convention, during which the NanoScan was used at the WESP outlet. The inlet aerosol concentration was again several orders of magnitude lower than the outlet. Further, the NanoScan and SMPS WESP outlet total aerosol concentration values were found to be very similar.

As with previous tests, the PSD for Test 8 showed a shift to very fine particulate and lower concentration. The NanoScan inlet PSD, however, was broad and shifted toward smaller aerosols, in contrast to the PSDs observed with the SMPS at the inlet in previous tests.

Test 9

Test 9 replicated conditions of Test 8, with a flow rate of 2700 acfm but a lower WESP current of 25 mA. During the first 2.5 hours of testing, the NanoScan sampled at the WESP inlet and the SMPS sampled at the WESP outlet, similarly to Test 8. The SMPS data appeared to be unreliable during this test as there was a large inexplicable dip in particulate measured shortly into the sample period, and the PSD was inconsistent with previous tests. The NanoScan was moved to the WESP to provide feed gas data at the end of the test, and the SMPS data were rejected. Comparing only the NanoScan aerosol concentrations, the trend of increasing particulate at the WESP outlet is consistent with values observed in previous tests.

The outlet particulate concentration was ~7 times higher (not quite an order of magnitude) relative to the inlet concentration. The NanoScan PSD for Test 9 showed a substantial shift in the WESP inlet PSD, with the maximum concentration occurring at ~30 nm, nearly identical to the WESP outlet aerosol PSD. Along with the unusual inlet PSD observed during Test 8, this result suggests that some change in the plant may have shifted the flue gas PSD at the WESP sampling location during Tests 8 and 9.

Dekati Stage Impactor Sampling

Particle-Size Distribution

A Dekati ELPI was used to collect particulate on substrate plates at the inlet and outlet to the WESP. The Dekati sampler consists of 15 stages of particulate collection ranging in size from 9.89 to 0.015 µm based on aerodynamic particle size. Particles recovered from each stage can be analyzed and weighed to determine mass loading.

Multiple ports at the WESP inlet and outlet allowed staged impactor sampling to be performed concurrent to SMPS/NanoScan sampling. The staged impactor measured larger-sized particulate up to 10 µm. Several of the Dekati 15-stage sample tests were continued overnight to provide long sample collection periods. The WESP was operated overnight and was minded by an engineer during these impactor sampling periods.

The staged impactor samples, collection periods, and aerosol concentrations are presented in Table 4, and the average inlet and outlet mass concentration results for these tests are shown in Table 5.

Figure 7 shows the PSDs for the two inlet tests based on recovered mass of captured particulate on each stage. The outlet aerosol loadings were too low to provide adequate PSDs. It should be noted that because the Dekati could sample much larger particulate than the SMPS or NanoScan could measure, the low overall mass loading at the WESP outlet does not contradict the

Table 4. Staged Impactor Sampling Periods and Aerosol Mass Concentrations

Test No.	Sample Location	Sample Date	Sample Time	Concentration, mg/Nm^3
1	WESP in	8/29 to 8/30	13:17–06:00	1.649
2	WESP in	9/3 to 9/4	18:26–12:27	1.164
3	WESP out	9/4 to 9/5	17:45–08:10	0.780
4	WESP out	9/5	10:02–17:09	0.280
5	WESP out	9/5 to 9/6	17:57–07:55	0.814

Table 5. Staged Impactor Average Aerosol Mass Concentration

Inlet, mg/Nm^3	Outlet, mg/Nm^3
1.407	0.625

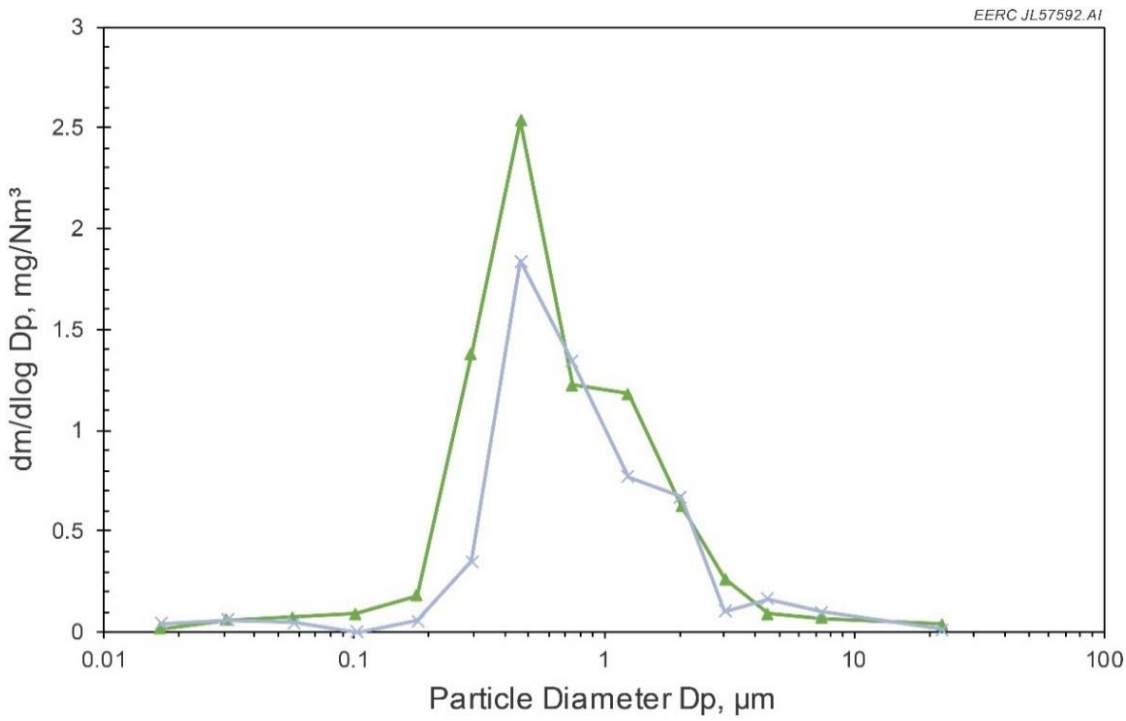

Figure 7. Dekati staged impactor inlet PSD.

mass increases measured at the WESP outlet by the SMPS or NanoScan. It is likely that the mass of very fine particulate measurable by the SMPS method was increasing through the WESP even as the total mass, including larger particulate not measurable by the SMPS, was being greatly reduced. This phenomenon can be due to oxidation of SO_2 to SO_3 across the WESP.

SEM Analysis of Impactor Stage Aerosols

Select substrates from the impactor stages were analyzed by scanning electron microscopy (SEM) analysis. Figure 8 presents chemistries for various metals collected on the impactor stages shown in the legend. Two SEM scans are presented for each stage analyzed to show potential variability in the aerosol composition.

Sulfur enrichment was present on all substrates, indicating possible sulfate or SO_3. The sulfate is likely originating from the MRY FGD in the form of $CaSO_3$. After normalization for sulfur content, Ca, Na, and K were enriched relative to the MRY ESP fly ash. Some metals (Cr, Mn) were perhaps traceable to stainless steel components.

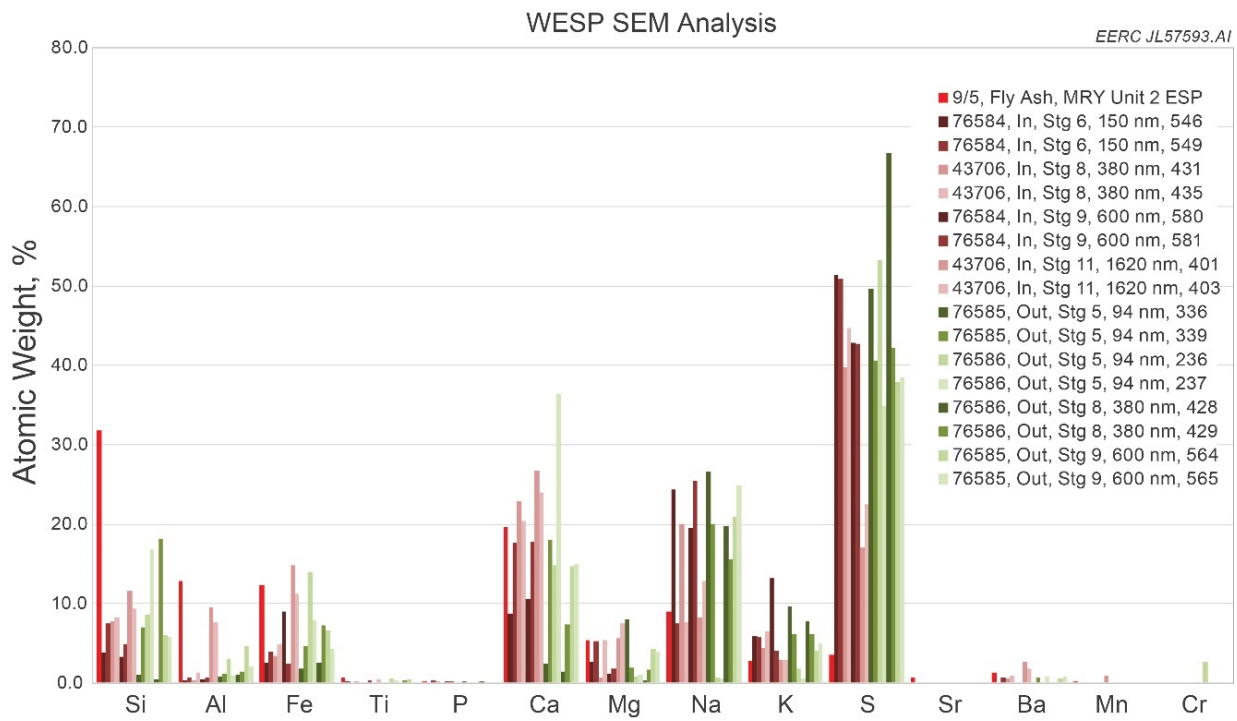

Figure 8. Aerosol chemistries obtained from SEM analysis.

SEM morphologies were gathered from the stages shown in Figure 8. There appear to be two distinct particle morphologies based on particle size. Figure 9 shows fly ash spheres captured on Stage 11 (1630 nm) of an inlet impactor test. At Stage 9 (600 nm), the inlet particulate appears to be more crystalline in shape, as shown in Figure 10.

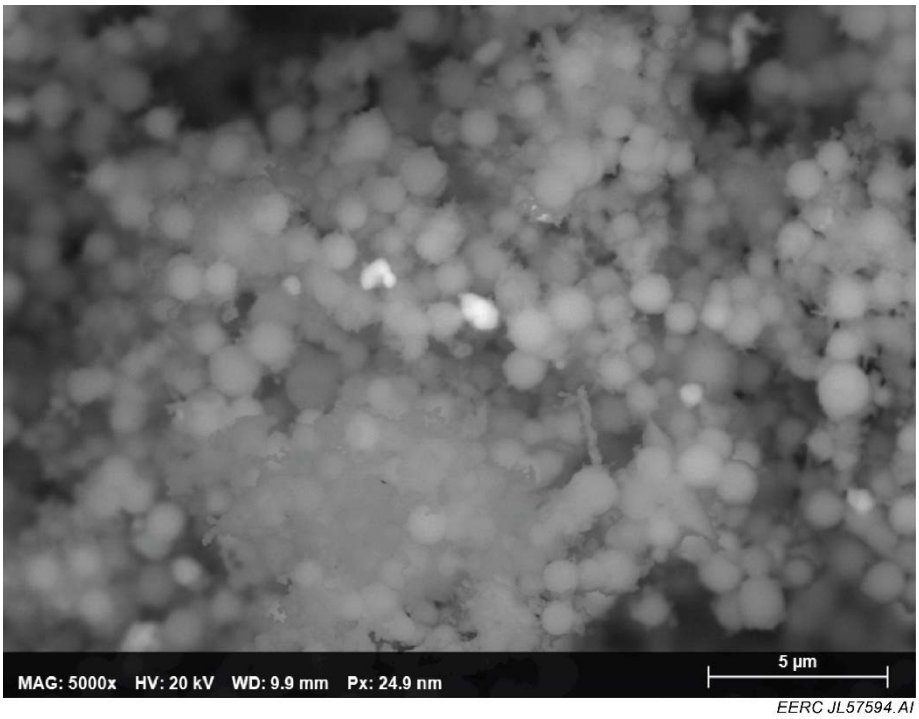

Figure 9. WESP inlet particle morphology from Dekati Stage 11 (1630 nm).

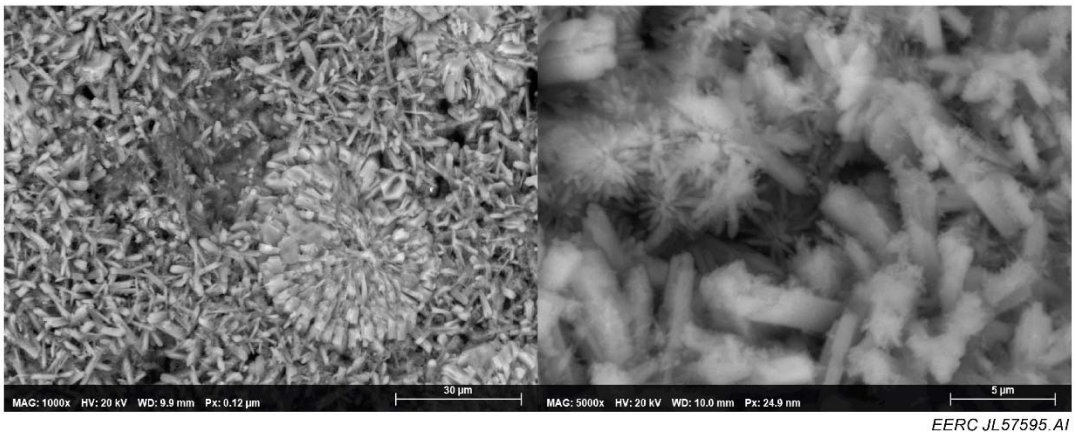

Figure 10. WESP inlet aerosol morphology from Dekati Stage 9 (603 nm).

SEM morphologies completed on WESP outlet stages did not exhibit the rod- or sliverlike particles seen at the inlet. The WESP outlet aerosol morphologies show very small spherical particles, and most appear to be embedded in a porous, spongelike arrangement. Figures 11 and 12 show select stages from WESP outlet aerosol morphologies.

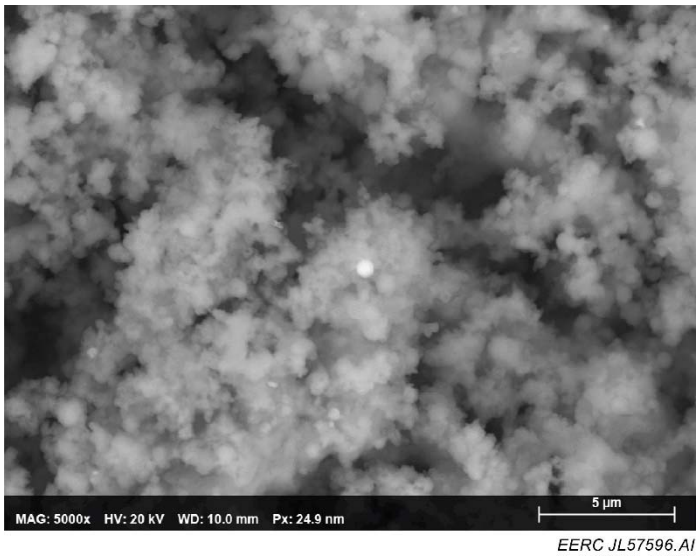

Figure 11. WESP outlet aerosol morphology for Stage 9 (603 nm).

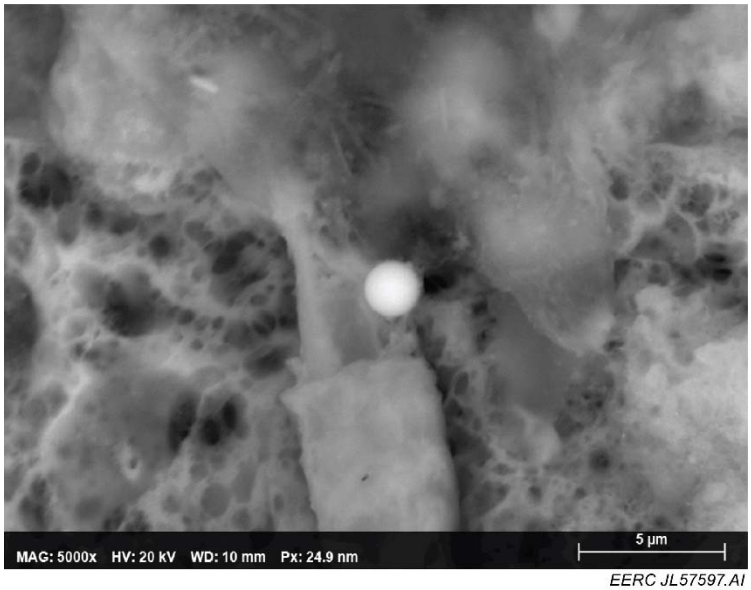

Figure 12. WESP outlet aerosol morphology for Stage 8 (382 nm).

ICP and ICP–MS Analysis of Impactor Stage Aerosols

The remaining, non-SEM-analyzed stage substrates from each of the five impactor tests were subjected to a leaching process to strip the bulk aerosols. The recovered solution was then analyzed via inductively coupled plasma (ICP) and ICP–mass spectroscopy (ICP–MS). These analyses were performed to estimate the bulk aerosol chemistry from all combined stages.

Figure 13 presents a bar chart of the elements in each substrate batch, normalized to a mass concentration (of aerosol) per volume of flue gas. Elements, where detected, were presented in the same order as those shown in the SEM results of Figure 8.

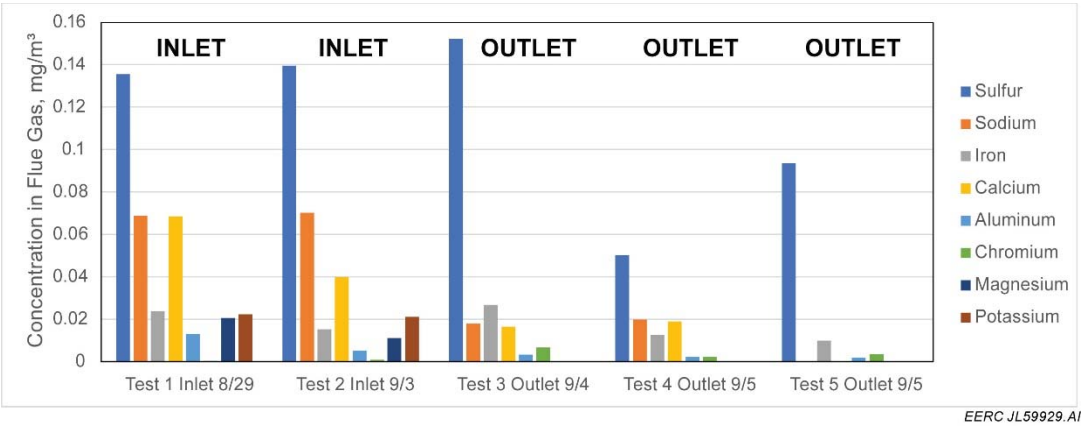

Figure 13. Bulk chemistry of WESP inlet and outlet substrates determined by ICP–MS.

Although the volume of leached solution (50 mL) was the same for each batch of substrates, the number of available substrates was different owing to the previous destructive loss via SEM. Consequently, a direct comparison of element concentration from test to test, and inlet versus outlet, should be considered semiquantitative for this analysis. The results indicated higher concentration of aluminum, calcium, and sodium for WESP inlet aerosol samples relative to outlet aerosol samples. Magnesium and potassium were also measured in inlet aerosols but were below detection in outlet samples.

WESP Specifications

Using the analytical results obtained from the rented WESP, MRY purchased a more optimized small-scale WESP that was installed upstream of the EERC's carbon capture system. This WESP included three parallel gas pathways through two electrical sequential fields, with each field activated independently.

Second-Phase Pilot-Scale Evaluations

The new WESP was received by MRY during the first quarter of 2020 and was installed in May 2020. Initial shakedown testing, conducted May 19–21, 2020, showed that the WESP could achieve better than 95% removal of fine particulate.

WESP Installation and Testing

To ensure proper operation of the WESP, a 3-day shakedown test was conducted on flue gas. A small-scale FGD, part of the existing EERC capture system, was also in operation and acted as a sulfur polisher scrubber. The capture system also included a DCC to control flue gas temperature

to the WESP and ultimately to the absorber column. During the initial shakedown, solvent was not in the absorber column. Operational parameters such as current and amperage control and wash down procedures were checked and verified. A Fourier-transform infrared (FTIR) instrument was used to sample the flue gas at the entrance and exit of the WESP, focusing on the concentrations of SO_2 and SO_3. A SMPS was also used to sample flue gas to determine the aerosol count in the flue gas at the inlet and outlet of the new WESP.

Aerosol-Sampling Results

During shakedown testing, sampling occurred with only one of the two electrical fields energized. Figure 14 gives the overall results of particle size and concentration from SMPS sampling across the WESP. Total aerosol particle counts measured at the inlet and outlet of the WESP are given in Table 6. Collection efficiency was calculated by taking the difference between the inlet and outlet concentration at each particle diameter and dividing by the inlet concentration. The calculated efficiency is given in Figure 15. Figure 16 gives the efficiency for the size range of 100 to 200 nm.

The discrepancy in the overall efficiency at the 700-nm range is most likely due to a short sampling time at the WESP inlet location and the very low particulate measured in this range. With few data points and a low concentration, small measurement errors or variabilities in particulate loading were amplified and led to dubious or even negative capture efficiencies for some of the larger particulate sizes. As can be seen in Figure 16, the WESP was very effective in removing aerosols in the range of 100 to 200 nm and did not show any of the increase in smaller particulate that had been previously observed with the rented WESP.

FTIR sampling results across the WESP are given in Figure 17. Initial data indicated that the WESP corona was not generating additional SO_3.

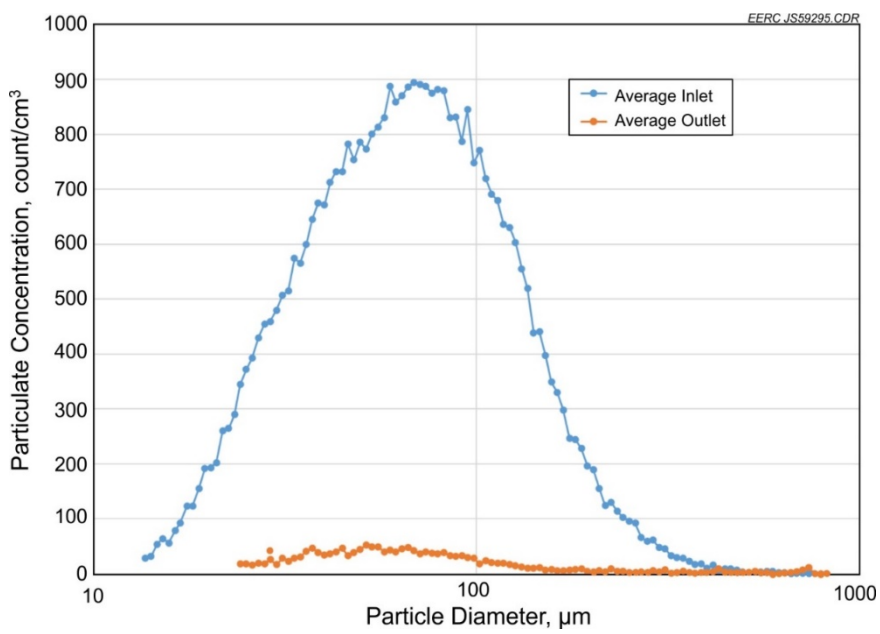

Figure 14. Overall size distribution and concentration as measured by the SMPS.

Table 6. Total Aerosol Particle Counts Measured at the Inlet and Outlet of the WESP

Parameter	WESP Inlet	WESP Outlet
Particle Concentration	4.1×10^4 particles/cm^3	2.1×10^3 particles/cm^3
Total Particles Counted	3.08×10^7 particles	2.19×10^6 particles

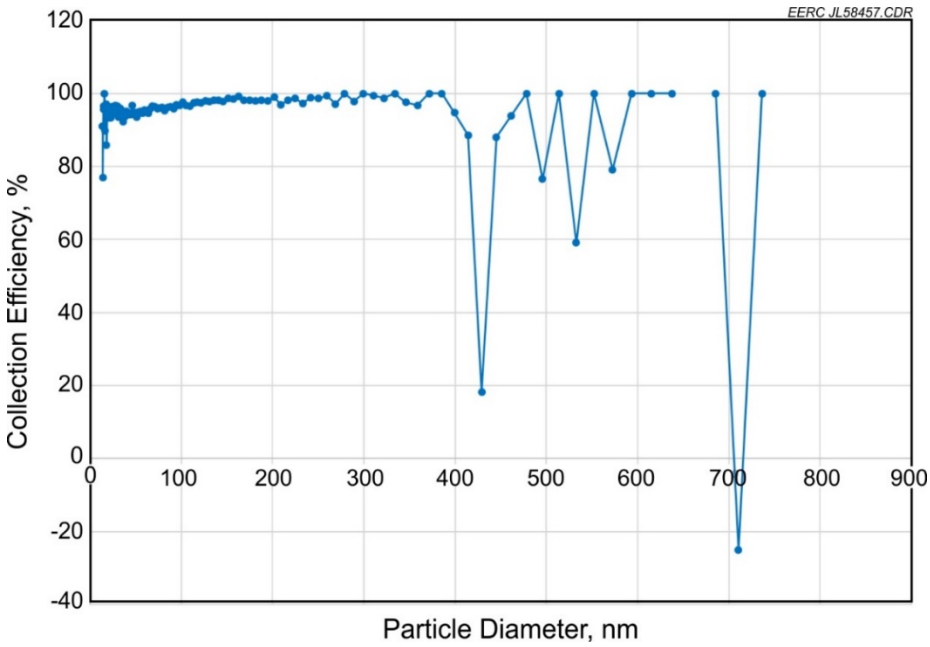

Figure 15. Overall calculated efficiency of the WESP.

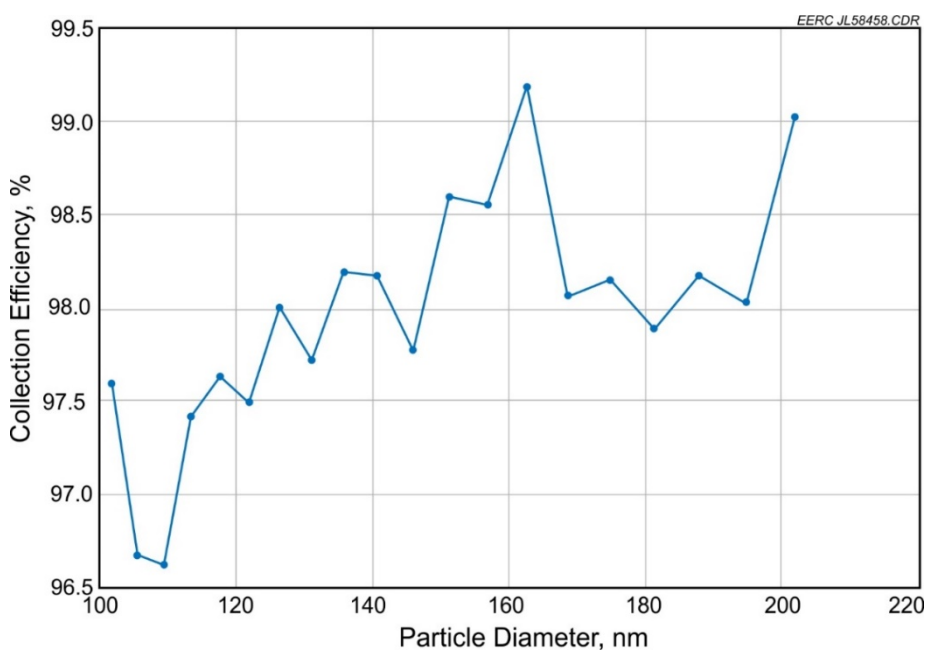

Figure 16. Calculated efficiency for the particle range of 100 to 200 nm.

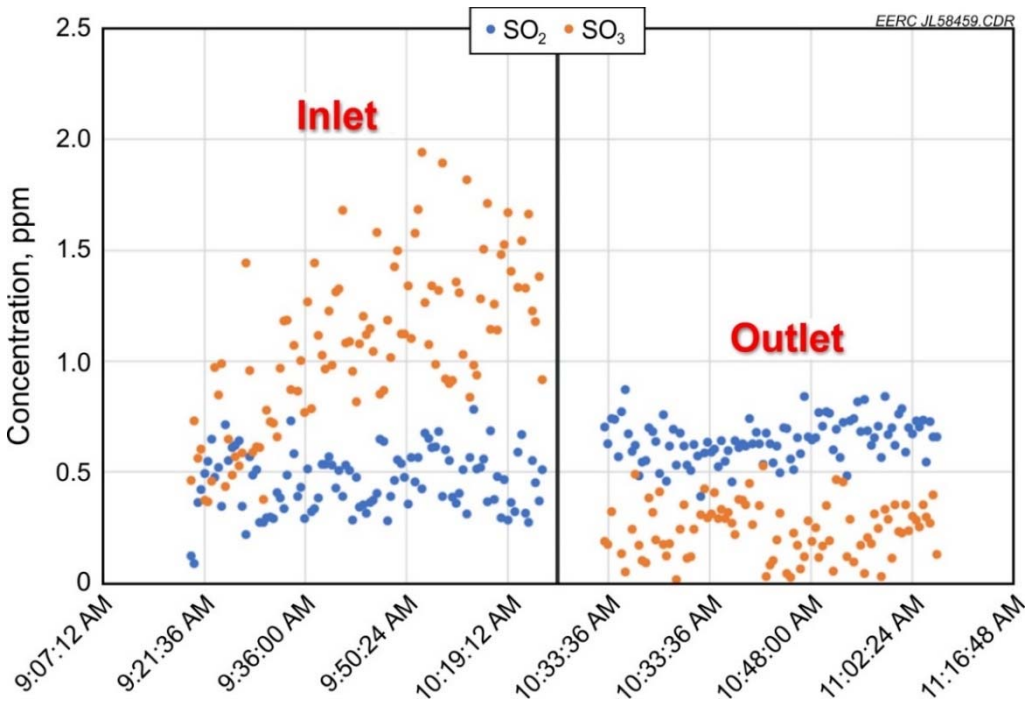

Figure 17. FTIR data at the inlet and outlet of the WESP.

Particulate loading across the scrubber and WESP in June 2020 indicated that the pilot-scale unit's scrubber and DCC were also contributing to particulate removal. As indicated in Figure 18, the particulate loading through the scrubber and DCC was reduced by an order of magnitude.

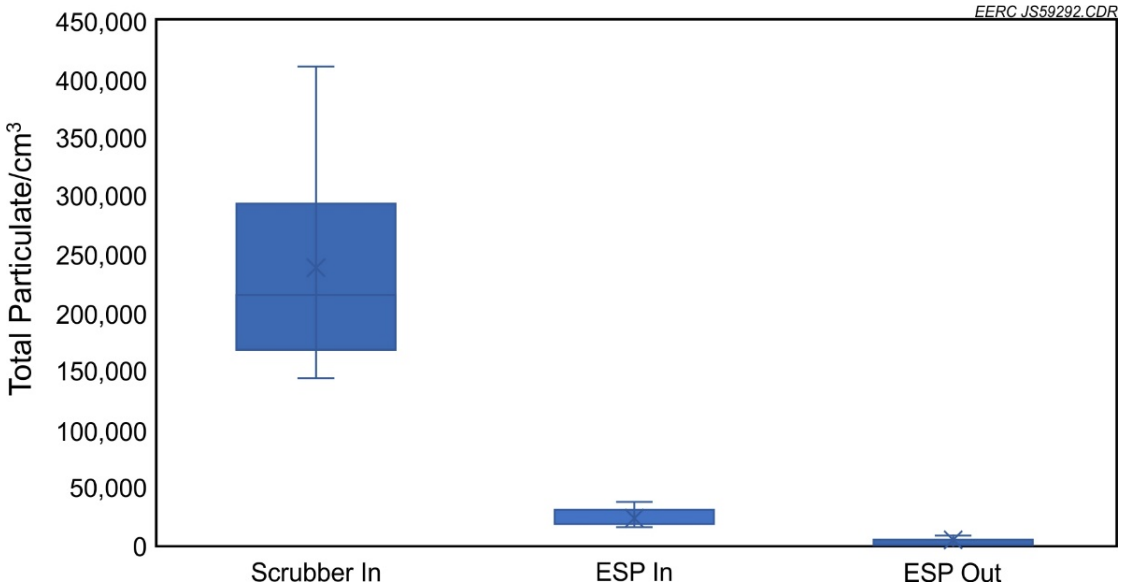

Figure 18. Total particulate at the scrubber inlet, WESP inlet, and WESP outlet during June 25 sampling.

Parametric Aerosol Testing

During operation of the capture system utilizing Fluor solvent, sampling was conducted across the entire test skid at the sampling points shown in Figure 19. Parametric testing was conducted to determine the significance of several variables in optimizing WESP performance. A set of factorial matrices were developed to maximize the information gathered while minimizing the time needed to perform the testing. The WESP parameters examined in the factorial matrices are as follows:

- Number of WESP fields online (0, 1, or 2)
- Voltage of WESP fields (15, 25, or 35 V)
- Inlet gas flow rate (100, 110, or 120 scfm)
- SO_2 concentration (either <2 ppm or >6 ppm)

While the first three variables could be adjusted as needed, SO_2 concentration could only be controlled by bringing the FGD and DCC columns online: When the FGD and DCC columns were both operating, nearly all SO_2 in the flue gas was captured; when the wet FGD was bypassed and the DCC column water flow was reduced, SO_2 at Sample Point 3 would rise closer to the level present at the inlet. Even with the FGD off-line, the DCC column captured some sulfur, so inlet sulfur to the WESP could never be increased completely to inlet levels. The DCC could not be turned off completely to allow greater sulfur slip because some cooling was necessary to control the CO_2 absorber inlet temperature.

Sampling was conducted using both the SMPS (for aerosol sampling) and the FTIR (for analysis of gas-phase sulfur speciation). Because the FTIR and the aerosol sampling utilize the same ports, sampling was completed separately. Aerosols were sampled at the outlet of the WESP over the course of 2 days (July 14 and 15) of parametric testing. Aerosols were then sampled at

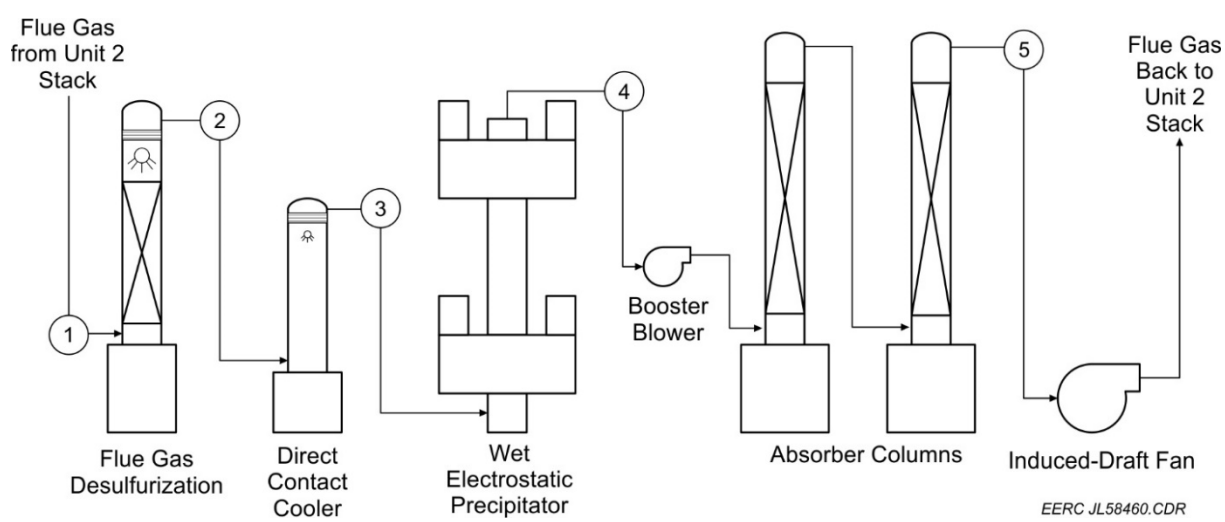

Figure 19. Schematic showing the gas path through the pilot test system. Numbered circles denote locations for gas sampling.

the outlet of the CO_2 absorber column on a third day (July 16) of parametric testing. The FTIR was used to sample the flue gas at the entrance and exit of the WESP over the course of 2 days (July 1 and 2), focusing on the concentrations of SO_2 and SO_3. FTIR sampling was then conducted at the outlet of the CO_2 absorber column on July 16. The test matrices for each sampling technique are given in Tables 7–10.

Table 7. Test Matrix for FTIR Sampling at the WESP Outlet

Test Order	Test Number	WESP Fields in Operation	WESP Field Voltage kV	Flue Gas Flow Rate scfm	SO_2 Polishing Scrubber Operation On/Off	SO_2 ppm	SO_3 ppm
1	Center point	One	25	110	On	0.58	2.19
2	WESP Washout						
3	1	None	–	110	On	0.65	2.40
4	7	None	–	120	On	0.63	2.56
5	Center point	One	25	110	On	0.63	2.60
6	4	Two	35	100	On	0.66	2.80
7	6	Two	15	120	On	0.81	1.23
8	8	Two	35	120	On	0.53	1.39
9	2	Two	15	100	On	0.67	2.00
10	WESP Washout						
11	Center point	One	25	110	On	0.83	1.75
12	3	None	–	100	On	0.79	1.84

Table 8. Test Matrix for FTIR Sampling at the Absorber Outlet

Test Order	Test Number	WESP Fields in Operation	WESP Field Voltage kV	Flue Gas Flow Rate scfm	SO_2 Polishing Scrubber Operation On/Off	SO_2 ppm	SO_3 ppm
1	Center point	One	25	110	On	0.97	1.71
2	**WESP Washout**						
3	1	None	–	110	On	0.97	1.18
4	7	None	–	120	On	0.88	1.02
5	Center point	One	25	110	On	0.93	1.43
6	4	Two	35	100	On	0.77	2.32
7	6	Two	15	120	On	1.02	2.00
8	8	Two	35	120	On	0.99	1.93
9	2	Two	15	100	On	1.10	2.01

Table 9. Test Matrix for Aerosol Sampling at the WESP Outlet

Test Order	Test Number	WESP Fields in Operation	WESP Field Voltage	Flue Gas Flow Rate	SO_2 Polishing Scrubber Operation	Total Particulate
			kV	scfm	On/Off	count/cm^3
1	Center point	One	25	110	On	5900
2				WESP Washout		
3	1	None	–	100	On	310,000
4	7	None	–	120	On	87,000
5	Center point	One	25	110	On	3200
6	4	Two	35	100	On	1300
7	6	Two	15	120	On	4200
8	8	Two	35	120	On	830
9	2	Two	15	100	On	5600
10				WESP Washout		
11	3	None	–	100	On	42,000
12	5	None	–	120	On	34,000
13	Center point	One	25	110	On	2500
14	Center point	One	25	110	Off	3600
15				WESP Washout		
16	3	None	–	100	Off	37,000
17	5	None	–	120	Off	36,000
18	2	Two	15	100	Off	350
19	8	Two	35	120	Off	190
20				WESP Washout		
21	Center point	One	25	110	Off	660

Table 10. Test Matrix for Aerosol Sampling at Absorber Outlet

Test Order	Test Number	WESP Fields in Operation	WESP Field Voltage	Flue Gas Flow Rate	SO_2 Polishing Scrubber Operation	Total Particulate
			kV	scfm	On/Off	count/cm^3
1	Center point	One	25	110	On	53
2				WESP Washout		
3	1	None	–	100	On	3700
4	7	None	–	120	On	1200
5	Center point	One	25	110	On	55
6	4	Two	35	100	On	200
7	6	Two	15	120	On	34
8	8	Two	35	120	On	190
9	2	Two	15	100	On	15

WESP Impacts on Aerosol and Sulfur Speciation

As illustrated in Figures 20 and 21, the only variable that had any statistically significant impact on particulate loading at the WESP outlet or the absorber outlet was having the WESP online. The difference in loading when using one or two fields was minimal, as was the effect of voltage, gas flow rate, or SO_2 loading. No variable had any discernable impact on FTIR results through the WESP. This shows that the WESP corona was not forming SO_3, as was speculated in the previous testing at higher SO_2 concentrations and observed by others (Laborelec, 2014).

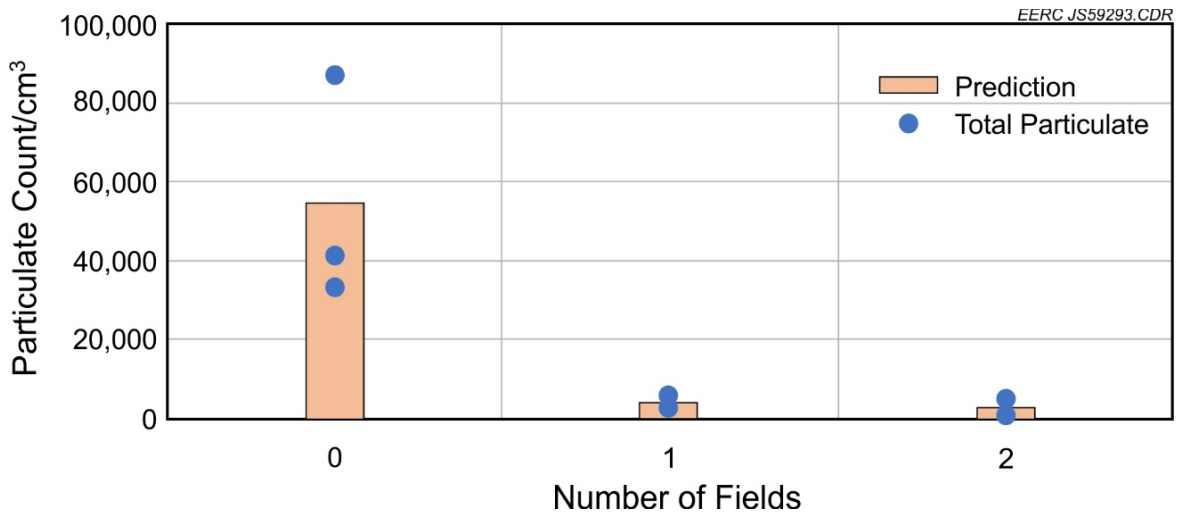

Figure 20. Particulate loading at the WESP outlet with SO_2 scrubber online.

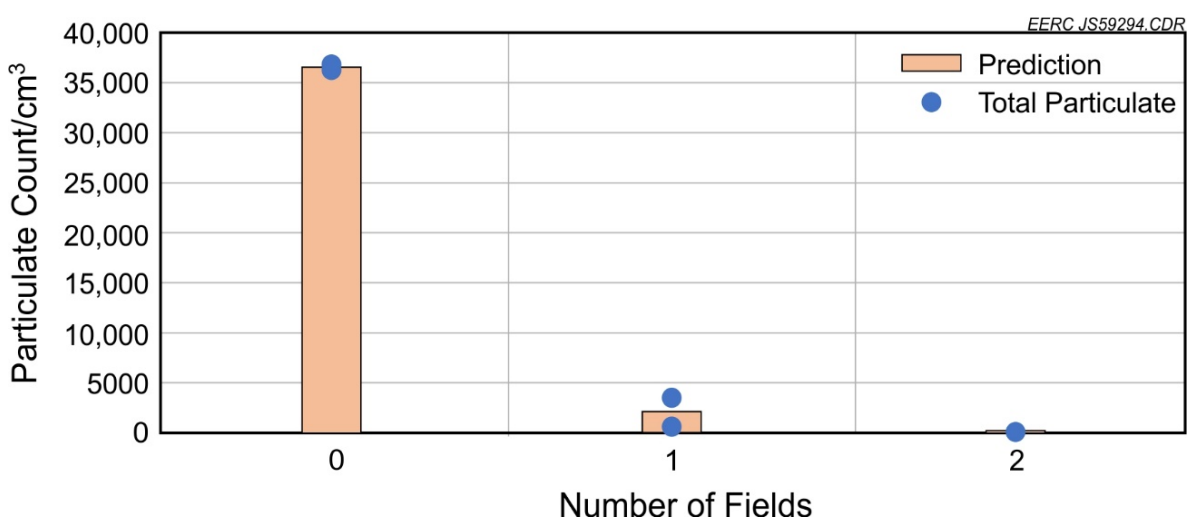

Figure 21. Total particulate loading at the WESP outlet with SO_2 scrubber off-line.

The results at the absorber outlet were similar, showing that the only parameter that impacted particulate loading was having the WESP online. Particulate loading at the absorber outlet was consistently lower than at the WESP outlet and shows that some of the particulate leaving the WESP was being removed through the CO_2 capture system. While the FTIR showed no change in gas-phase speciation through the WESP, the FTIR showed an increase in NH_3 and a reduction in SO_3 through the CO_2 absorber columns. High amine losses have been observed in previous testing with this column, which does not have a water wash section at the top. SO_3 losses likely correspond to a slow increase in sulfates observed in the solvent analysis.

During SMPS sampling, it was observed that particulate measurements at the WESP inlet were higher during the morning than in the afternoon. This is especially clear when considering the center points in Table 9—Tests 1, 5, and 13—which are all the same and were all taken on July 14. These tests show decreasing particulate as the day progresses, as do Tests 14 and 21, which were taken on July 15. Examining all data taken at either the WESP inlet or with the WESP off-line, there appears to have been a diurnal cycle in particulate loading from morning to afternoon, as illustrated in Figure 22. SMPS data suggest that this cycle mostly affects the very fine particulate or aerosols (<100 nm). The cause of this cycle remains unknown, as does whether this diurnal cycle is a regular occurrence, but the trend shows that flue gas particulate exiting a lignite-fired power plant can vary strongly throughout the course of the day.

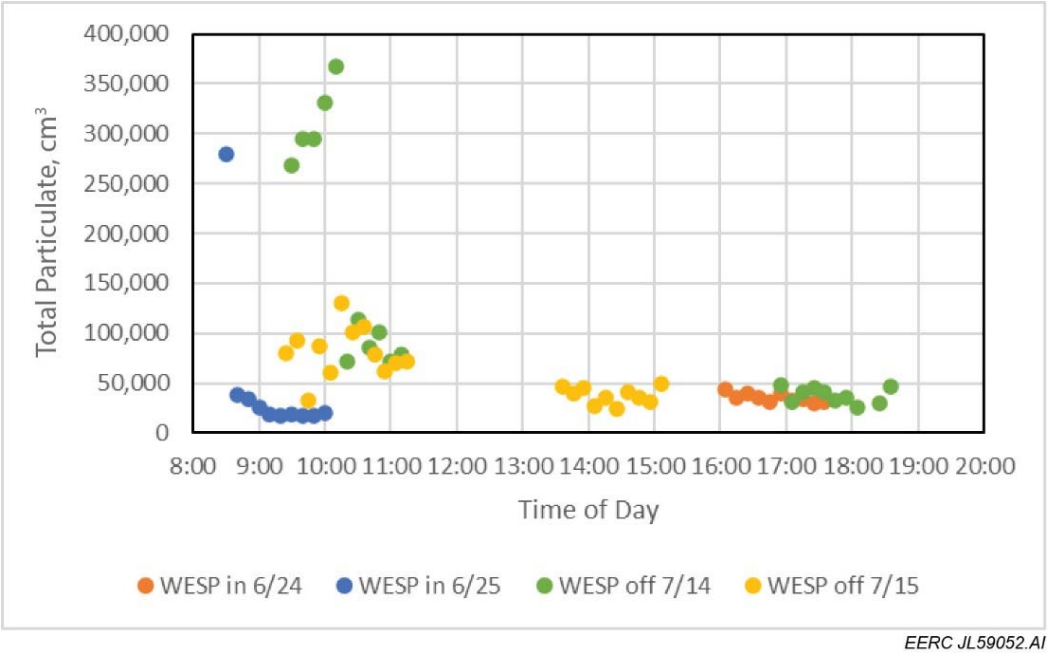

Figure 22. Total particulate count by hour of day without the WESP.

Dekati Sampling

Long-term particulate samples were taken from the inlet and outlet to the WESP using the Dekati ELPI. Substrates were recovered after 12 hours of exposure to gas and weighed to estimate particulate loading. The recovered substrates were then analyzed by field emission scanning electron microscope (FESEM) to assess particle type and makeup. A portion of each substrate was dissolved into solution for chemical analysis by ICP and ICP–MS.

Dekati Substrate Analysis

So little particulate was collected at the WESP outlet that the weight gain could not be reliably measured. At the inlet, the PSD was similar between June 25 and July 14, with the bulk of the particulate being in Stage 7 (mean diameter = 0.257 µm), as illustrated in Figure 23. It should be noted that the Dekati data are expressed on a weight basis, while the SMPS data were expressed in number of particles, so the PSDs have different shapes and peaks. Based on Dekati analyses, the total particulate loading at the WESP inlet is estimated at 0.924 to 1.213 mg/Nm^3.

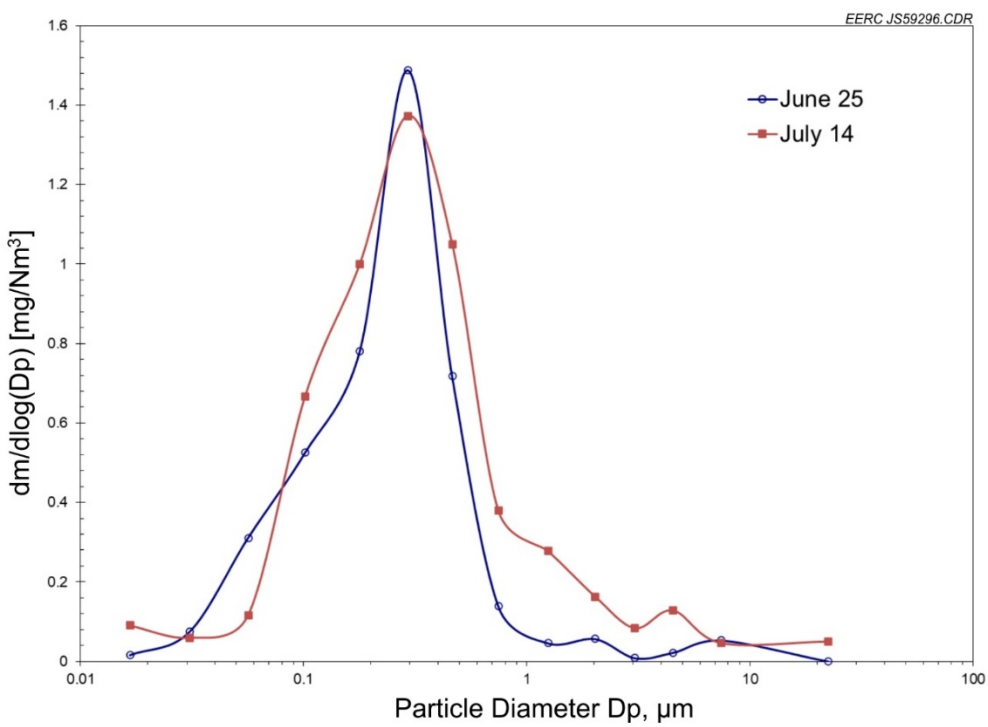

Figure 23. PSDs at WESP inlet as determined by Dekati measurements.

Substrates from Stage 7 of the Dekati sampling test at the inlet of the WESP were analyzed by FESEM to obtain morphological images and to estimate elemental chemistry. FESEM chemical results for Stage 7 are shown in Figure 24. The chemical analysis shows a high concentration of sulfur in conjunction with significant amounts of Na, K, and Ca. The presence of these elements indicates that much of the particulate consisted of alkali and alkaline-earth sulfates.

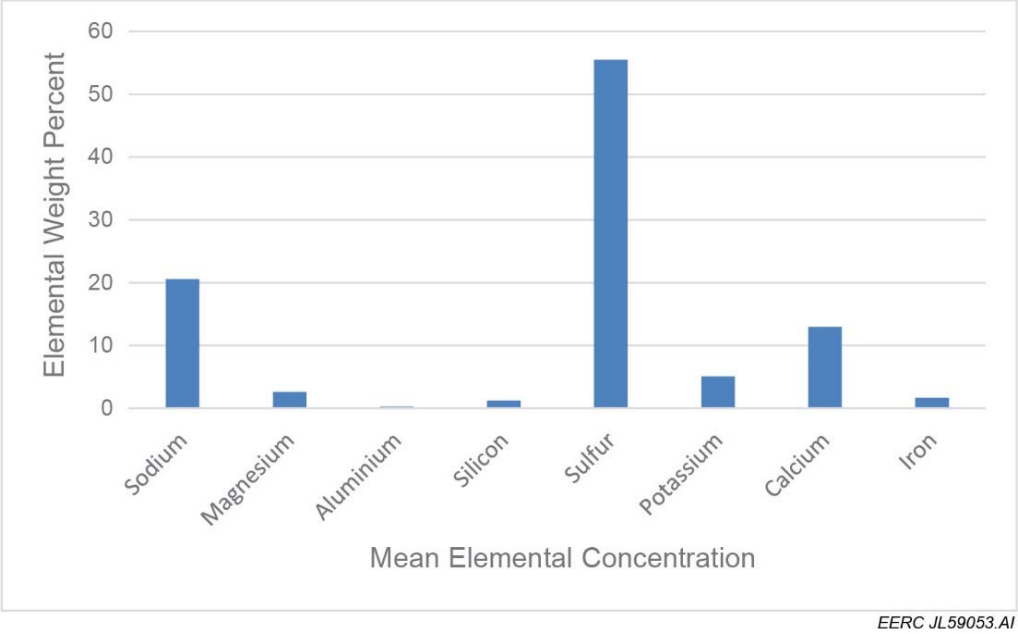

Figure 24. Mean elemental chemical analysis of the particulate collected on Stage 7 of the Dekati.

Each Dekati substrate was cut in half, and one half of each was digested into 50 mL of solution to be analyzed by ICP and ICP–MS. During initial WESP screening discussed earlier, the substrates submitted for FESEM analysis could no longer be digested and did not contribute to the ICP–MS analysis. Only half of each substrate was submitted for FESEM when analyzing data from the new WESP to ensure that a representative digestive sample could be prepared from all substrates collected. For each test condition, substrates from all stages were generally combined into a single solution. Results are shown in Figure 25.

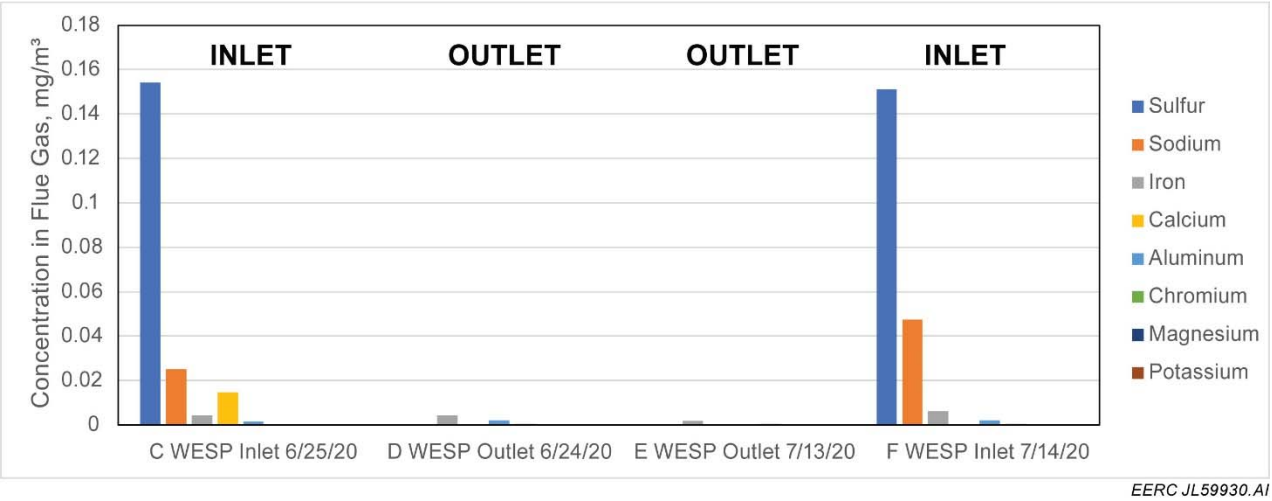

Figure 25. Metal concentrations in solutions of digested Dekati substrates.

Samples C and F were both taken at the WESP inlet, and both solutions of digested substrate contained high levels of sulfur and sodium. Sample C also contained appreciable calcium. This is in agreement with the FESEM assessment shown in Figure 24. By contrast, Samples D and E were taken at the WESP outlet, and both solutions contained no detectable sulfur, sodium, or calcium. It should be noted that the FTIR showed no change in gas-phase sulfur concentration or speciation through the WESP during any of the parametric testing. These results suggest that much of the particulate-borne sulfate was being captured by the WESP without release of SO_3.

FESEM image analysis showed that the particulate collected at the WESP inlet in 2020, after flue gas had passed through a secondary FGD and DCC, was substantially different than the particulate collected in 2019, when flue gas was sampled directly from the plant's FGD unit outlet. In the 2019 testing, the inlet gas to the WESP was found to contain significant carryover from the plant's FGD unit. FESEM analysis of the Dekati substrates taken at the WESP inlet in 2019 had identified numerous crystalline particles as calcium sulfite (refer to Figure 10). No crystalline material was present at the WESP inlet in 2020, as shown in Figure 26.

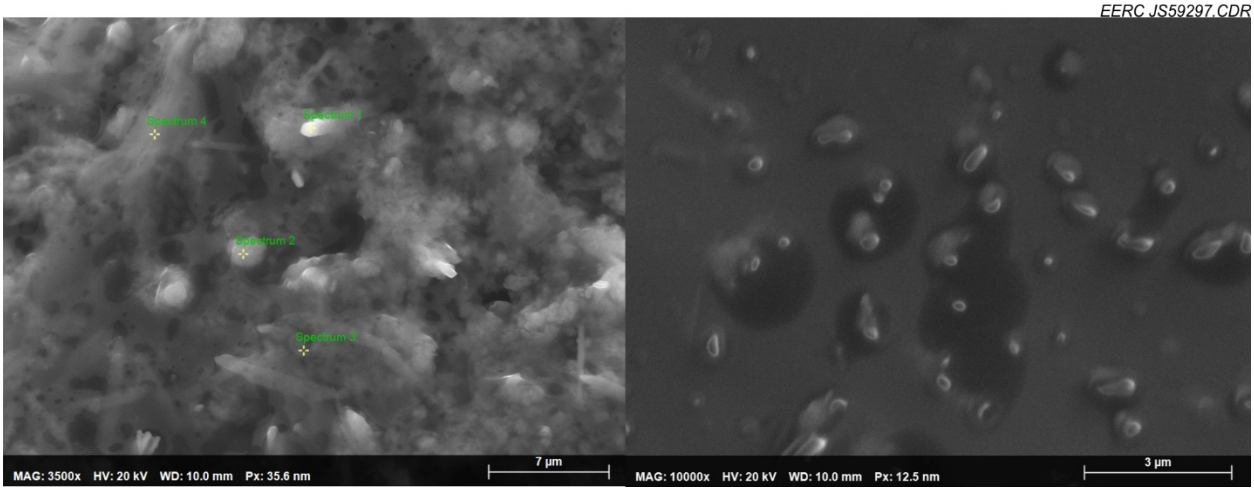

Figure 26. WESP inlet morphology from Stages 7 and 15.

Solvent Analysis

Testing with Fluor solvent began on June 17, 2020, and continued through July 17, 2020. Solvent samples were collected at the start of testing and then after every 5 days of operation. The recovered solvents were analyzed by ICP and ICP–MS for major cations, trace elements, anions, and HSS. The list of analytes is given in Table 11. The solvent samples were also analyzed for total inorganic carbon (TIC), reflecting the amount of CO_2 remaining absorbed in the solvent, and for acidity, providing a reflection of the amine content.

Table 11. Solvent Constituents Analyzed by ICP/ICP–MS

Constituent	Expected Concentration Range
Aluminum	150–800 ppb
Arsenic	1–110 ppb
Calcium	Not detected
Chromium	5–500 ppb
Cobalt	15–50 ppb
Copper	50–45,000 ppb
Iron	200–5500 ppb
Magnesium	Not detected
Manganese	5–50 ppb
Mercury	< 0.2 ppb
Nickel	Not detected – 600 ppb
Potassium	0.2–10 ppm
Selenium	1–50 ppb
Silicon	Not detected – 5 ppm
Sodium	0.5–20 ppm
Vanadium	5–50 ppb
Zinc	250–35,000 ppb
Acetate	< 0.5 ppm
Bromide	Not detected – 20 ppm
Chloride	Not detected – 10 ppm
Formate	Not detected – 150 ppm
Fluoride	< 0.5 ppm
Nitrate	Not detected – 500 ppm
Nitrite	Not detected – 50 ppm
Oxalate	Not detected – 50 ppm
Sulfate	Not detected – 150 ppm
Thiosulfate	1–5 ppm

Figures 27–30 show changes in concentrations through the test duration. For major cations, the solvent showed initial spikes in calcium and magnesium in the first week that then seemed to drop off gradually. Silicon and sodium did not exhibit this initial spike but continued to slowly rise throughout the test.

Many of the trace metals exhibited the same initial spike seen for calcium and magnesium. These include cobalt, vanadium, nickel, manganese, iron, and zinc. These metals may be associated with the stainless steel used to construct the system. Several of the other trace elements generally increased with time of exposure. These include lead, chromium, selenium, and possibly copper.

The concentrations of anions and HSS all tended to rise throughout the test duration. The lean solvent TIC (not charted) also increased slightly throughout the test period. While most of these materials rose gradually, the sulfate content jumped roughly sixfold in the last sample.

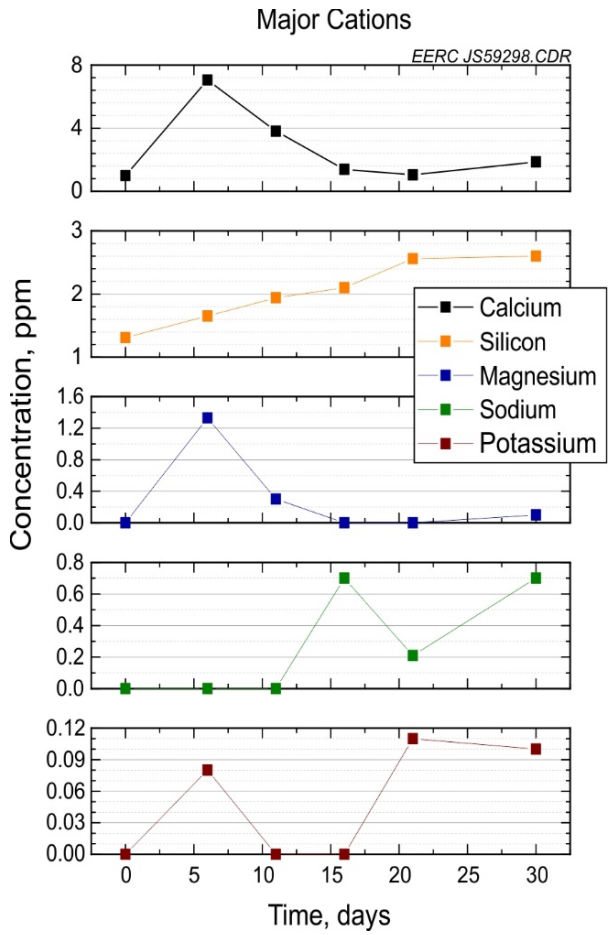

Figure 27. Concentrations of major cations in the solvent.

In addition to sulfate, calcium and sodium also rose slightly between the last two samples, which were taken on July 8 and July 17. This may correspond to the parametric testing conducted on July 14, 15, and 16, when both the FGD and the WESP were taken off-line for extended durations. The jumps in concentration are in agreement with analytical results from the Dekati substrates in Figures 24 and 25, which showed that the fine particulate at the WESP inlet was rich in sodium and calcium sulfate. This material would have passed directly to the absorber column during periods with the WESP off-line during parametric testing. FTIR results similarly showed a drop in gas-phase SO_3 through the absorber columns as the amine solution reacted with gas-phase SO_3. During normal operation, the total concentration of gas-phase sulfur at the column inlet was around 1 ppm or lower, but the gas-phase sulfur concentration was higher when the inlet FGD unit was taken off-line on July 15.

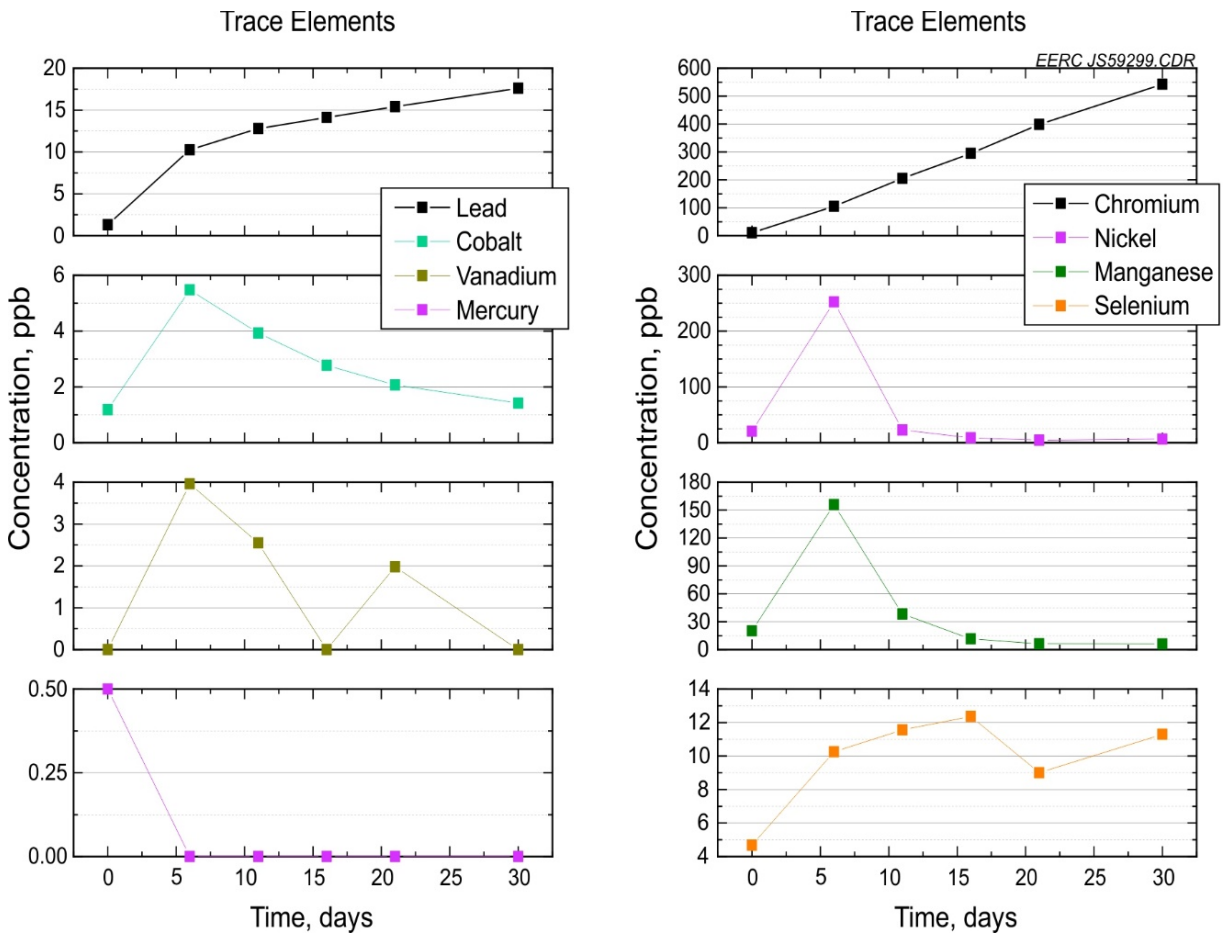

Figure 28. Concentrations of trace elements (Pb, Co, V, Hg, Cr, Ni, Mn, Se) in the solvent.

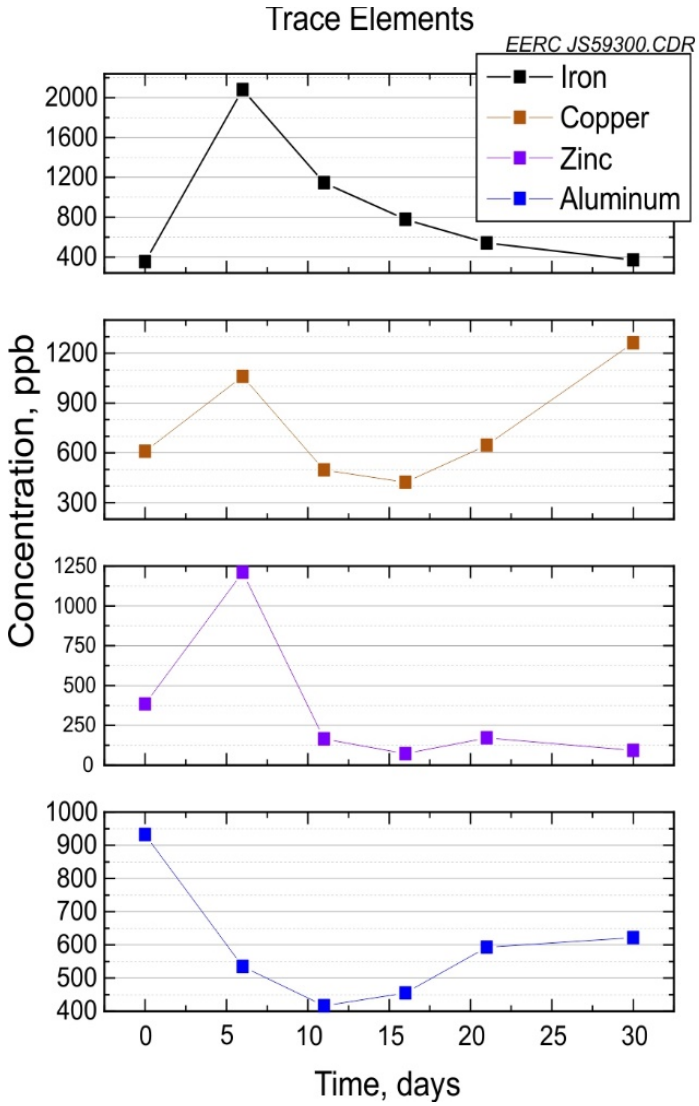

Figure 29. Concentrations of trace elements (Fe, Cu, Zn, Al) in the solvent.

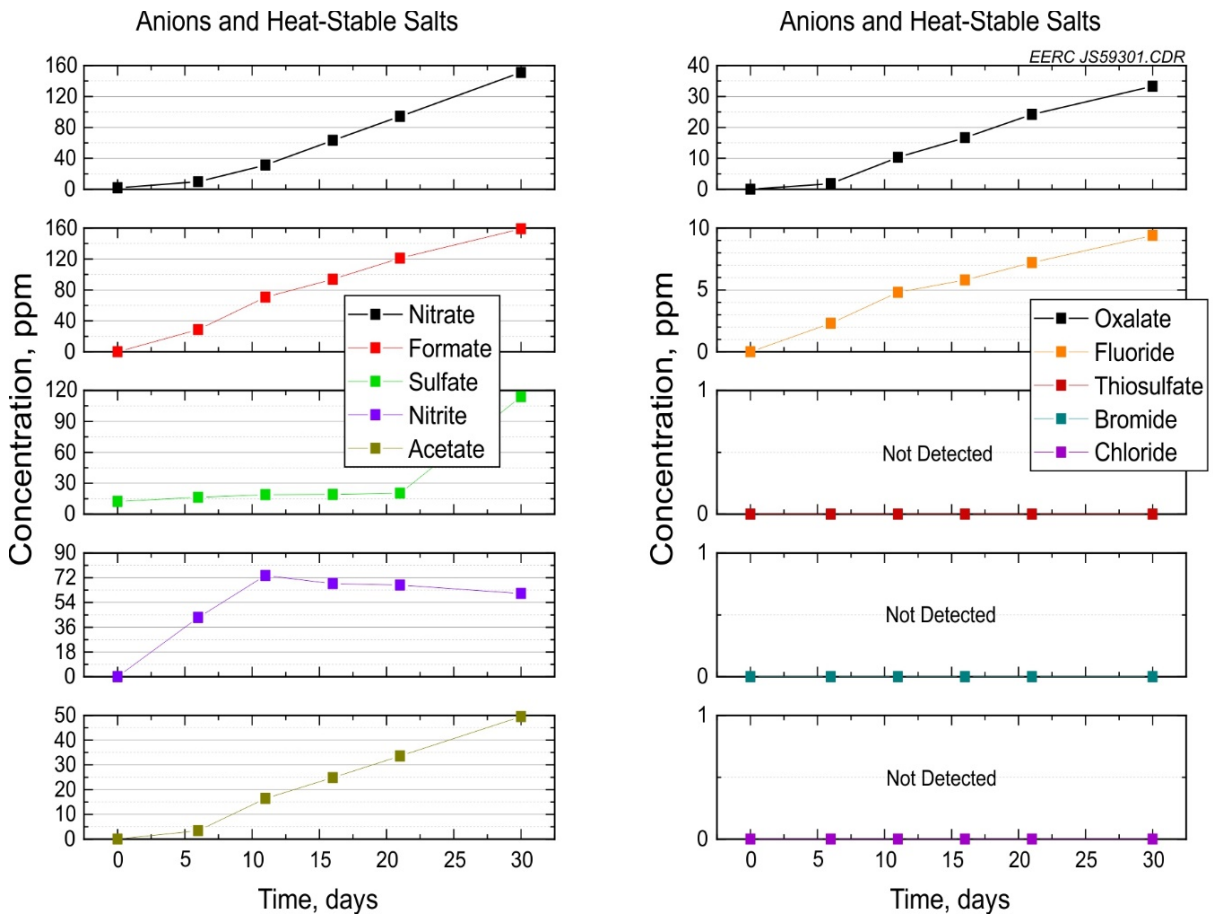

Figure 30. Concentrations of anions and HSS in the solvent.

Although Figures 27 through 30 show a gradual accumulation of several species that may be of concern for solvent degradation, it should be stressed that the levels observed may not be problematic. Solvent vendors would need to determine whether any of the trends are reason for concern. Based on the EERC's previous experience in amine-based CO_2 capture, the concentrations are low for this length of exposure time and should be manageable through solvent reclaiming.

CONCLUSIONS

Without adequate upstream gas conditioning, calcium sulfite carryover exiting the full-scale FGD passed directly to the rented WESP and converted to fine aerosols and SO_3. This tendency for the WESP operated in higher SO_2 concentrations to generate fine aerosols in sizes below ~75 nm was observed under every set of conditions studied, with very little variation in the outlet particulate loading. For fine particulate measurable by SMPS, the total particulate mass loading was unchanged or slightly increased under every set of conditions studied.

Dekati analysis of the particulate collected at the inlet and outlet of the rented WESP showed that the WESP was effective at reducing the total mass of larger particulate matter. This is not contradictory to the fine particulate results, because the SMPS and NanoScan instruments measure a much smaller size fraction than does the Dekati impactor. Samples collected at the WESP inlet contained fibrous and crystalline calcium sulfite materials that were not present in samples collected at the WESP outlet. Spherical and amorphous particulates were observed at both the inlet and outlet to the WESP.

When used downstream of an additional FGD polishing scrubber and DCC, the new special-built WESP reduced particulate from above 35,000 to <5000 count/cm^3. Dekati substrate analysis showed that the particulate at the WESP inlet contained appreciable alkali and alkaline-earth sulfates. This material was readily captured by the WESP, and the corona did not generate SO_3. Changing the number of fields, voltage, flow, or SO_2 had no statistically significant impact on WESP performance, and no variable had any impact on gas composition as measured by FTIR across the WESP.

The inlet FGD unit and WESP were effective at limiting the amount of sulfur and fine particulate at the absorber column inlet. Measurements at the absorber outlet showed that the amine solvent was also removing some of the sulfur and particulate that slipped through, leading to a gradual accumulation of several cations, trace elements, anions, and HSS in the solvent. After the FGD and WESP units were taken off-line to conduct parametric testing, the concentration of sulfate in the solvent jumped appreciably. This sudden jump in sulfate, along with smaller jumps in calcium and sodium, demonstrates that the inlet gas treatment configuration had a significant impact on reducing potential amine-based solvent degradation which, in turn, would be expected to extend solvent life.

MILESTONES

The completed milestone table can be found in Table 12.

Table 12. Milestones

Milestone Title/ Description	Planned Completion Date	Actual Completion Date	Verification Methods	Comments
M1 – Initiate Field Tests	11/1/19	9/23/19	Reported in subsequent quarterly report.	
M2 – Identify WESP Parameters	2/1/20	1/31/20	Reported in subsequent quarterly report.	

REFERENCES

Agalliu, I.; Smith, C.; Tavallali, M.; Rao, M.; Adams, S.; Montero, A.; Levesque, L.; Coughlin, C.; Yang, D.; Gallagher, S. *CO_2 EOR Potential in North Dakota: Challenges, Policy Solutions and Contribution to Economy and Environment*; Consulting Report; IHS Energy: June 2016, www.legis.nd.gov/files/committees/64-2014%20appendices/IHS%20Energy%20-%20Final%20Report.pdf (accessed Sept 19, 2019).

Brachert, L.; Mertens, J.; Khakharia, P.; Schaber, K. The Challenge of Measuring Sulfuric Acid Aerosols: Number Concentration and Size Evaluation Using a Condensation Particle Counter (CPC) and an Electrical Low Pressure Impactor (ELPI+). *J. Aerosol Sci.* **2014**, *67*, 21–27.

Chen, X.; Freeman, S.A.; Rochelle, G.T. Foaming of Aqueous Piperazine and Monoethanolamine for CO_2 Capture. *Int. J. Greenh.* **2011**, *5*, 381–386.

Cuzuel, V.; Gouedard, C.; Cuccia, L.; Brunet, J.; Rey, A.; Dugay, J.; Vial, J.; Perbost-Prigent, F.; Ponthus, J.; Pichon, V.; Carrette, P.-L. Amine Degradation in CO_2 Capture. 4. Development of Complementary Analytical Strategies for a Comprehensive Identification of Degradation Compounds of MEA. *Int. J. Greenh.***2015**, *42*, 439–453.

Dutcher, B.; Fan, M.; Russell, A.G. Amine-Based CO_2 Capture Technology Development from the Beginning of 2013 – A Review. *ACS Appl. Mater. Interfaces* **2015**, *7*, 2137−2148.

Fulk, S.M. Measuring and Modeling Aerosols in Carbon Dioxide Capture by Aqueous Amines. Ph.D. Dissertation, University of Texas at Austin, 2016.

Fytianos, G.; Ucara, S.; Grimstvedtb, A.; Hyldbakkb, A.; Svendsena, H.F.; Knuutila, H.K. Corrosion and Degradation in MEA-Based Postcombustion CO_2 Capture. *Int. J. Greenh.* **2016**, *46*, 48–56.

Goff, G.S.; Rochelle, G.T. Monoethanolamine Degradation: O_2 Mass Transfer Effects under CO_2 Capture Conditions. *Ind. Eng. Chem. Res.* **2004**, *43*, 6400–6408.

Gouedard, C.; Picq, D.; Launay, F.; Carrette, P.-L. Amine Degradation in CO_2 Capture. I. A Review. *Int. J. Greenh.***2012**, *10*, 244–270.

Gouedard, C.; Rey, A.; Cuzuel, V.; Brunet, J.; Delfort, B.; Picq, D.; Dugay, J.; Vial, J.; Pichon, V.; Launay, F.; Assam, L.; Ponthus, J.; Carrette. P.-L. Amine Degradation in CO_2 Capture. 3. New Degradation Products of MEA in Liquid Phase: Amides and Nitrogenous Heterocycles. *Int. J. Greenh.***2014**, *29*, 61–69.

Kamijo, T.; Sorimachi, Y.; Shimada, D.; Miyamoto, D.; Endo, T.; Nagayasu, H.; Mangiaracina, A. Result of the 60 tpd CO_2 Capture Pilot Plant in European Coal Power Plant with KS-1™ Solvent. *Energy Procedia* [online] **2013**, *37*, 813–816.

Khakharia, P. Aerosol-Based Emission, Solvent Degradation, and Corrosion in Post-Combustion CO_2 Capture. Ph.D. Dissertation, Technische Universiteit Delft, 2015.

Khakharia, P.; Brachert, L.; Mertens, J.; Anderlohr, C.; Huizinga, A.; Sanchez Fernandez, E.; Schallert, B.; Schaber, K.; Vlugt, T.J.H.; Goetheer, E. Understanding Aerosol-Based Emissions in a Post-Combustion CO_2 Capture Process: Parameter Testing and Mechanisms. *Int. J. Greenh.* **2015**, *34*, 63–74.

Khakharia, P.; Brachert, L.; Mertens, J.; Huizingaa, A.; Schallert, B.; Schaber, K.; Vlugt, T.; Goetheer, E. Investigation of Aerosol-Based Emission of MEA Due to Sulphuric Acid Aerosol and Soot in a Post-Combustion CO_2 Capture Process. *Int. J. Greenh.* **2013**, *19*, 138–144.

Khakharia, P.; Mertens, J.; Vlugt, T.J.H.; Goetheer, E. Predicting Aerosol Based Emissions in a Post-Combustion CO_2 Capture Process Using an Aspen Plus Model. *Energy Procedia* **2014a**, *63*, 911–925.

Khakharia, P.; Huizinga, A.; Jurado Lopez, C.; Sanchez, C.; de Miguel, Mercader, F.; Vlugt, T.J.H.; Goetheer, E. Acid Wash Scrubbing as a Countermeasure for Ammonia Emissions from a Postcombustion CO_2 Capture Plant. *Ind. Eng. Chem. Res*. **2014b**, *53*, 13195–13204.

Kittel, J.; Gonzalez, S. Corrosion in CO_2 Post-Combustion Capture with Alkanolamines – A Review. *Oil Gas Sci. Technol. – Revue IFP Energies Nouv*. **2014**, *69*, 915–929.

Laborelec, R.; A Wet Electrostic Precipitator (WESP) as Countermeasure to Mist Formation in Amine Based Carbon Capture. In International Journal of Greenhouse Gas Control; Elsevier: Linkebeek, Belgium, 2014; pp 175–181.

Laumb, M.; Benson, S.; Kay, J.; McCollor, D.; Bowman, F.; Sisk, D. *Assessment of Particulate Characteristics Upstream and Downstream of ESP and Wet FGD*; Final Report for Minnkota Power Cooperative, Inc.; July 1, 2009.

Le Moullec, Y.; Neveux, T.; Al Azki, A.; Chikukwa, A.; Hoff, K.A. Process Modifications for Solvent-Based Post-Combustion CO_2 Capture. *Int. J. Greenh.* **2014**, *31*, 96–112.

Luis, P. Use of Monoethanolamine (MEA) for CO_2 Capture in a Global Scenario: Consequences and Alternatives. *Desalination* **2016**, *380*, 93–99.

Mertens, J.; Brachert, L.; Desagher, D.; Thielens, M.L.; Khakharia, P.; Goetheer, E.; Schaber, K. ELPI+ Measurements of Aerosol Growth in an Amine Absorption Column. *Int. J. Greenh.* **2014**, *23*, 44–50.

Mertens, J.; Lepaumier, H.; Desagher, D.; Thielens, M. Understanding Ethanolamine (MEA) and Ammonia Emissions from Amine-Based Post-Combustion Carbon Capture: Lessons Learned from Field Tests. *Int. J. Greenh.***2013**, *13*, 72–77.

Nickolic, H.; Frimpong, R.A.; Liu, K. Trace Metals Accumulation in a Coal-Fired Postcombustion CO_2 Capture Process with Amine-Based Solvents. *Int. J. Greenh.* **2015**, *42*, 59–65.

Rey, A.; Gouedard, C.; Ledirac, N.; Cohen, M.; Dugay, J.; Vial, J.; Pichon, V.; Bertomeu, L.; Picq, D.; Bontemps, D.; Chopin, F.; Carrette, P.-L. Amine Degradation in CO_2 Capture. 2. New Degradation Products of MEA. Pyrazine and Alkylpyrazines: Analysis, Mechanism of Formation and Toxicity. *Int. J. Greenh.* **2013**, *19*, 576–583.

Schallert, B.; Neuhaus, S.; Satterley, C.J. Do We Underestimate the Impact of Particles in Coal-Derived Flue Gas on Amine-Based CO_2 Capture Processes? *Energy Procedia* **2013**, *37*, 817–825.

Schallert, B.; Neuhaus, S.; Satterley, C.J. Is Fly Ash Boosting Amine Losses in Carbon Capture from Coal? *Energy Procedia* **2014**, *63*, 1944–1956.

Veltman, K.; Singh, B.; Hertwich, E.G. Human and Environmental Impact Assessment of Postcombustion CO_2 Capture Focusing on Emissions from Amine-Based Scrubbing Solvents to Air. *Environ. Sci. Technol.* **2010**, *44*, 1496–1502.

Wu, X.; Yu, Y.; Qin, Z.; Shang, Z. The Advances of Post-Combustion CO_2 Capture with Chemical Solvents: Review and Guidelines. *Energy Procedia* **2014**, *63*, 1339.

APPENDIX A

PARTICULATE TEST DATA FROM RENTED WESP

PARTICULATE TEST DATA FROM RENTED WESP

TEST 1

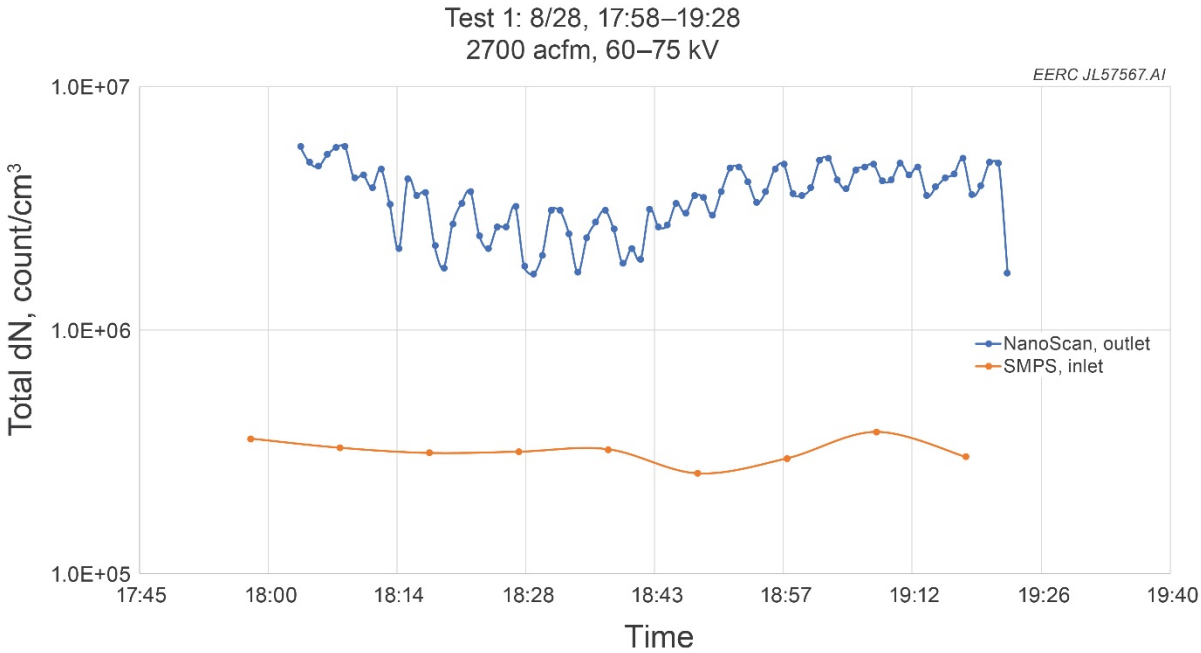

Figure A-1. Test 1 total aerosol concentration.

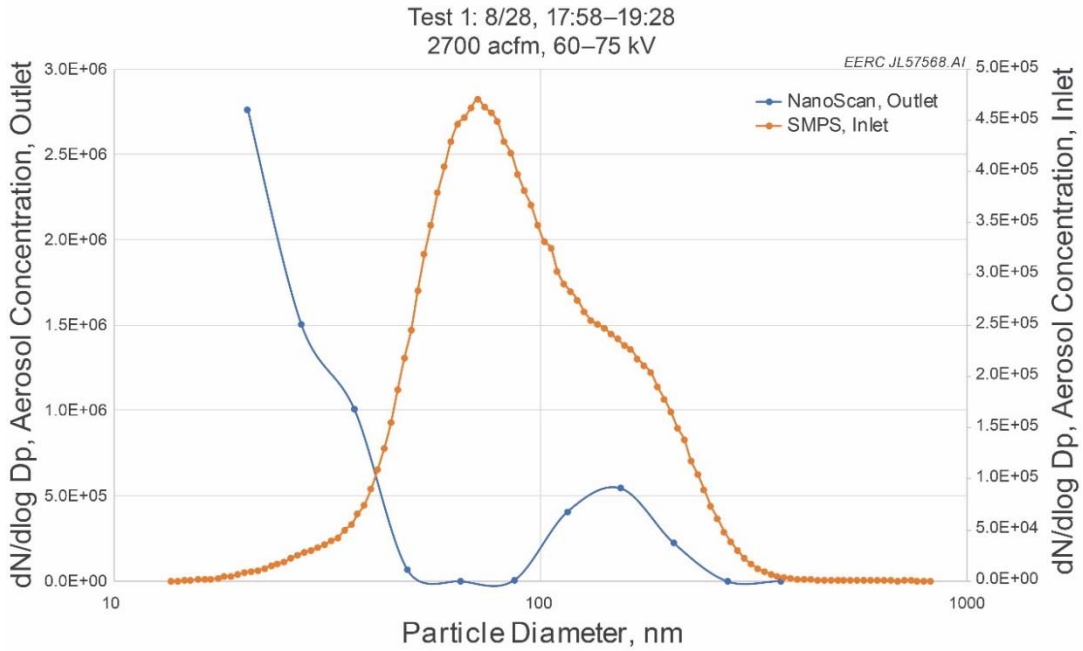

Figure A-2. Test 1 average particle-size distribution (PSD).

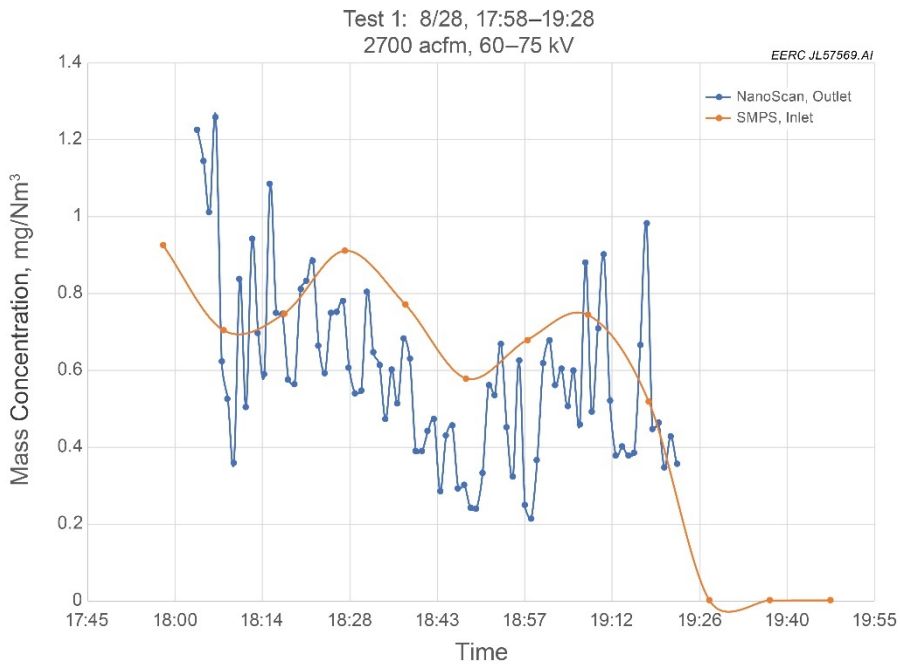

Figure A-3. Test 1 aerosol mass concentration.

TEST 2

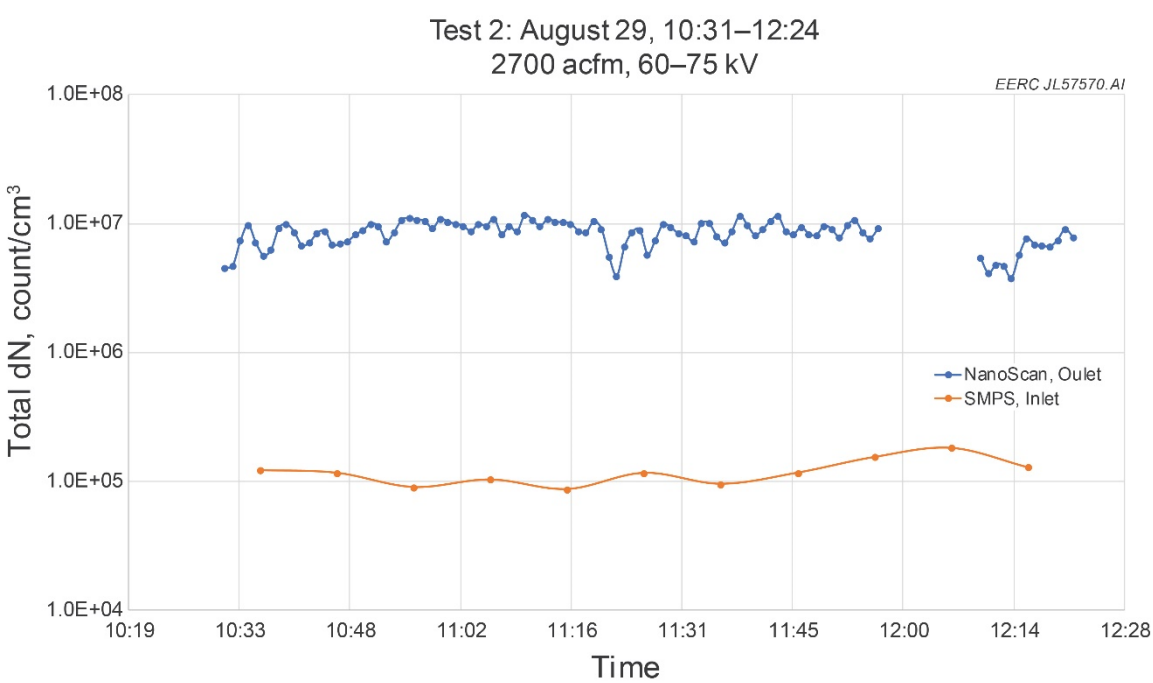

Figure A-4. Test 2 total aerosol concentration.

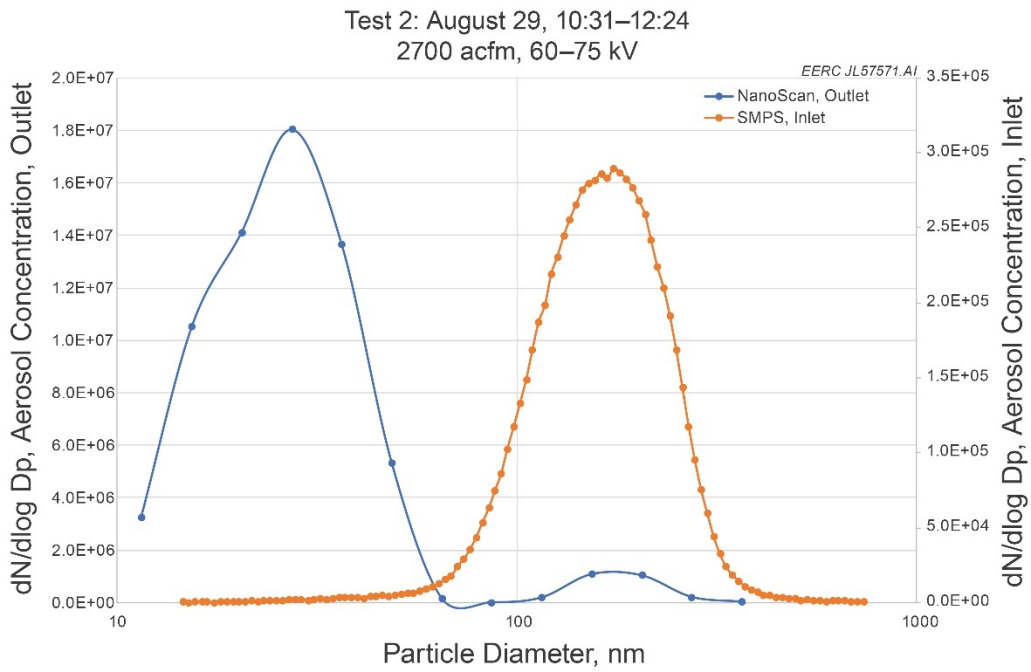

Figure A-5. Test 2 average PSD.

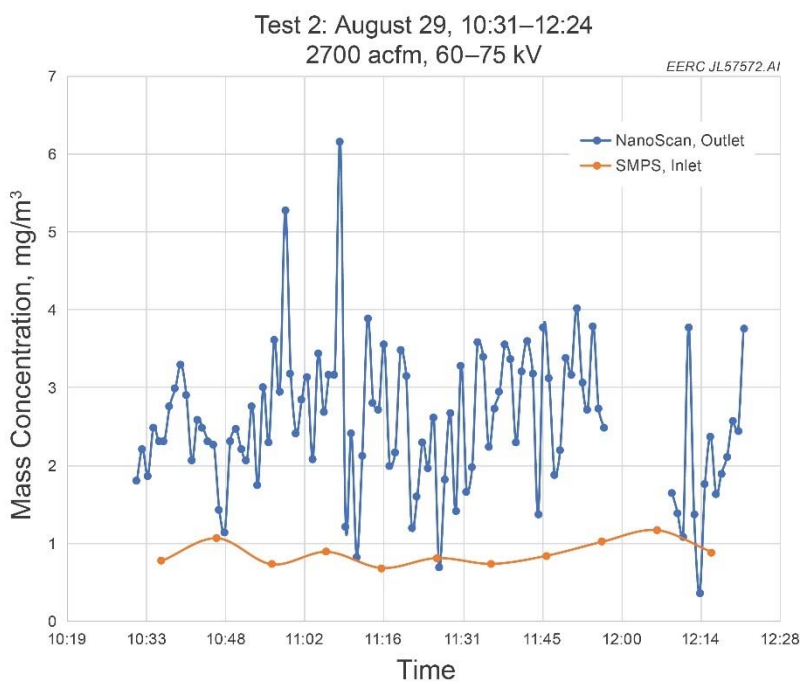

Figure A-6. Test 2 aerosol mass concentration.

TEST 3

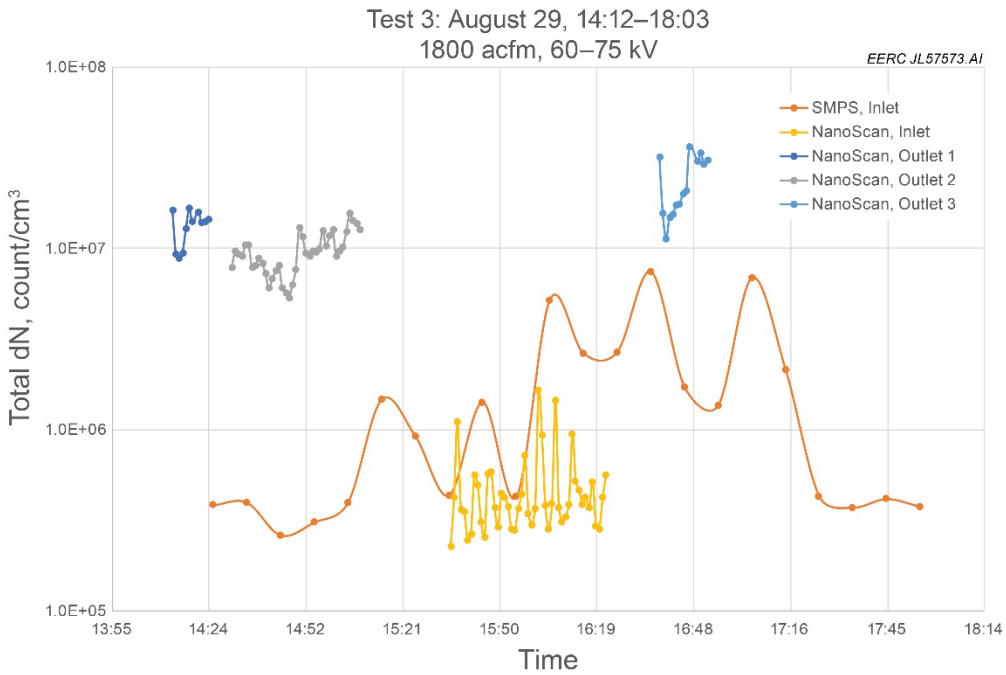

Figure A-7. Test 3 total aerosol concentration.

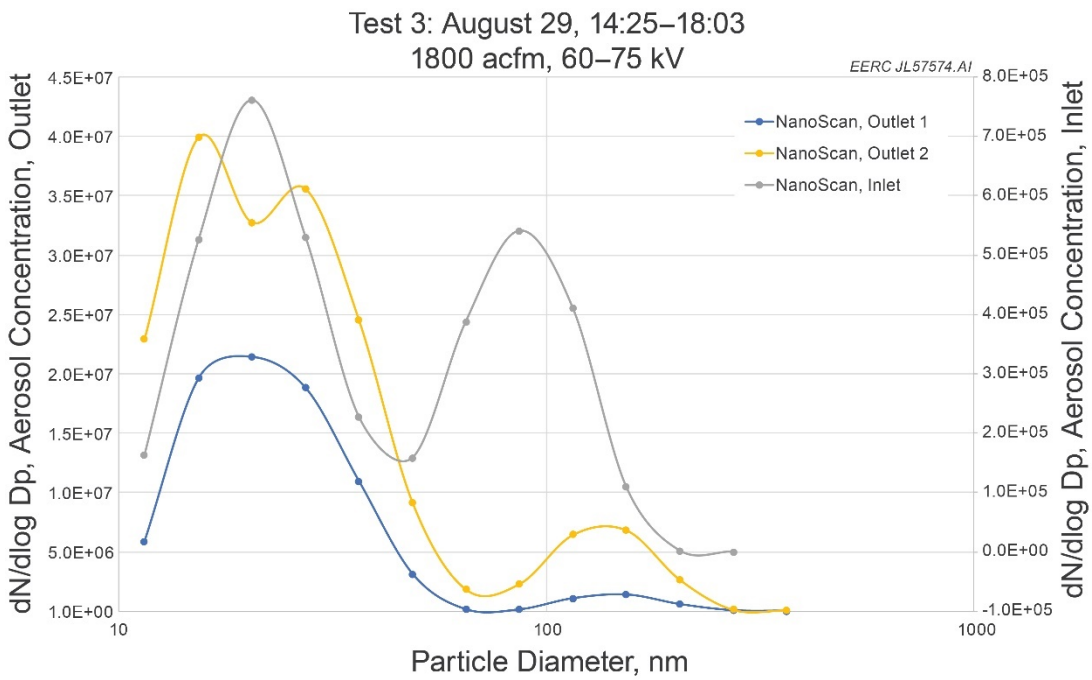

Figure A-8. Test 3 average PSD.

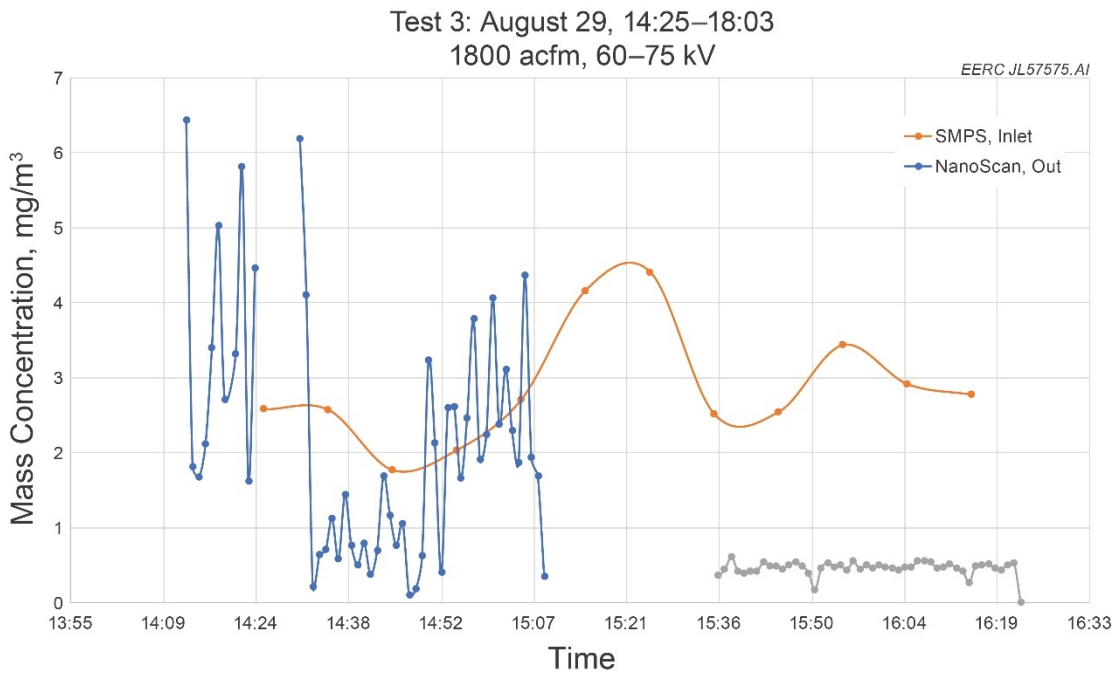

Figure A-9. Test 3 aerosol mass concentration.

TEST 4

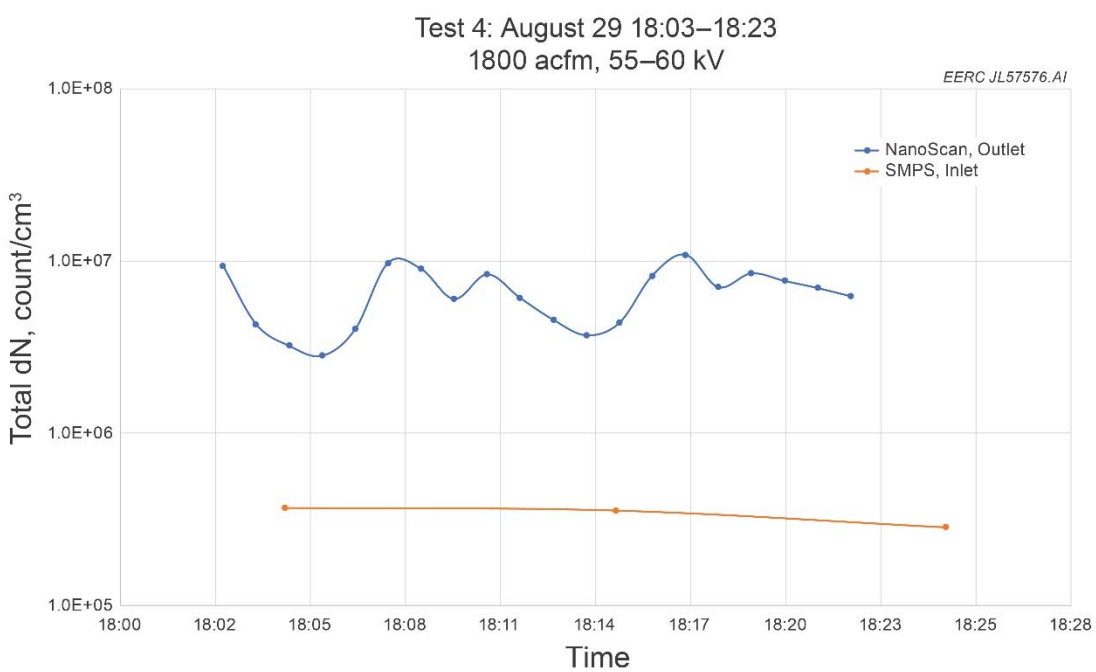

Figure A-10. Test 4 total aerosol concentration.

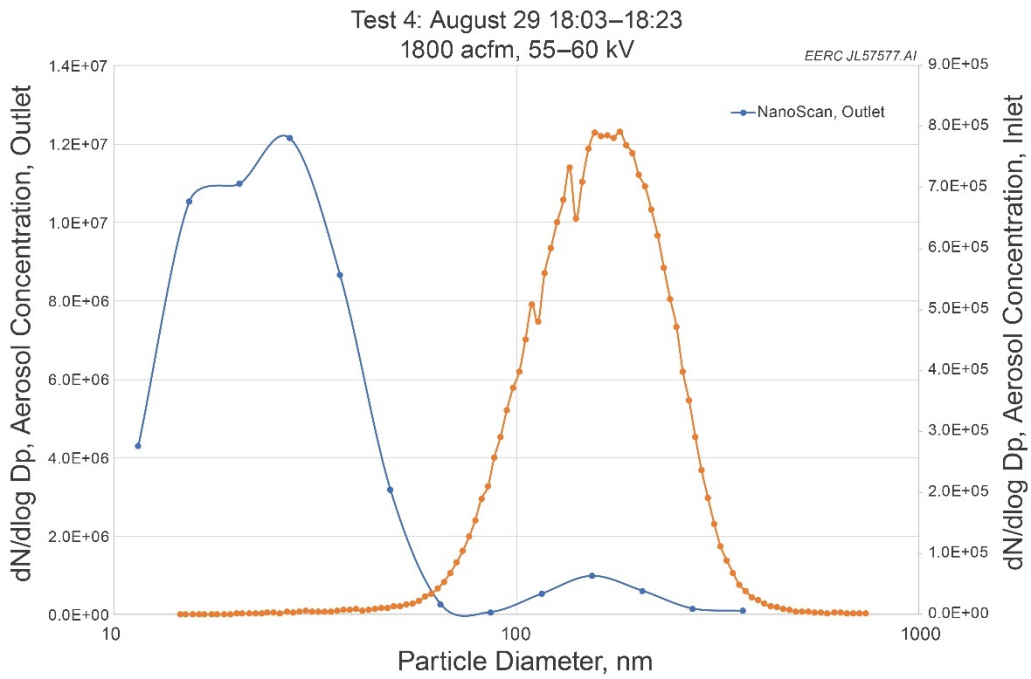

Figure A-11. Test 4 average PSD.

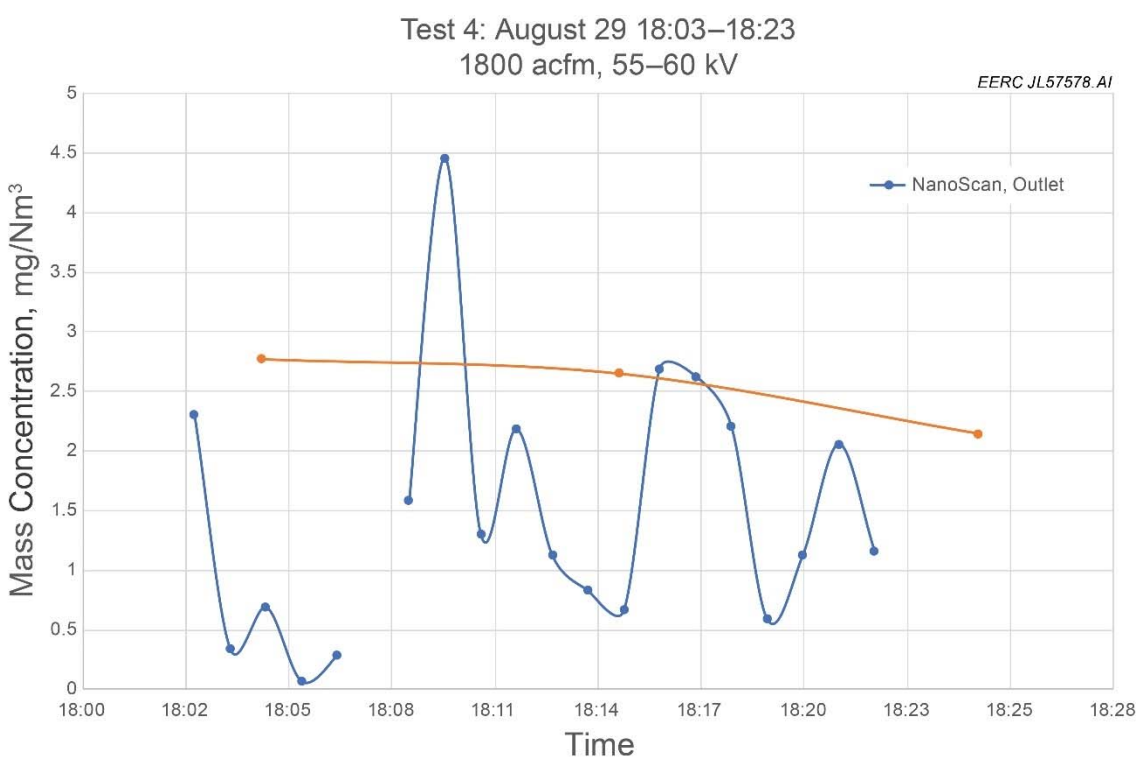

Figure A-12. Test 4 aerosol mass concentration.

TEST 5

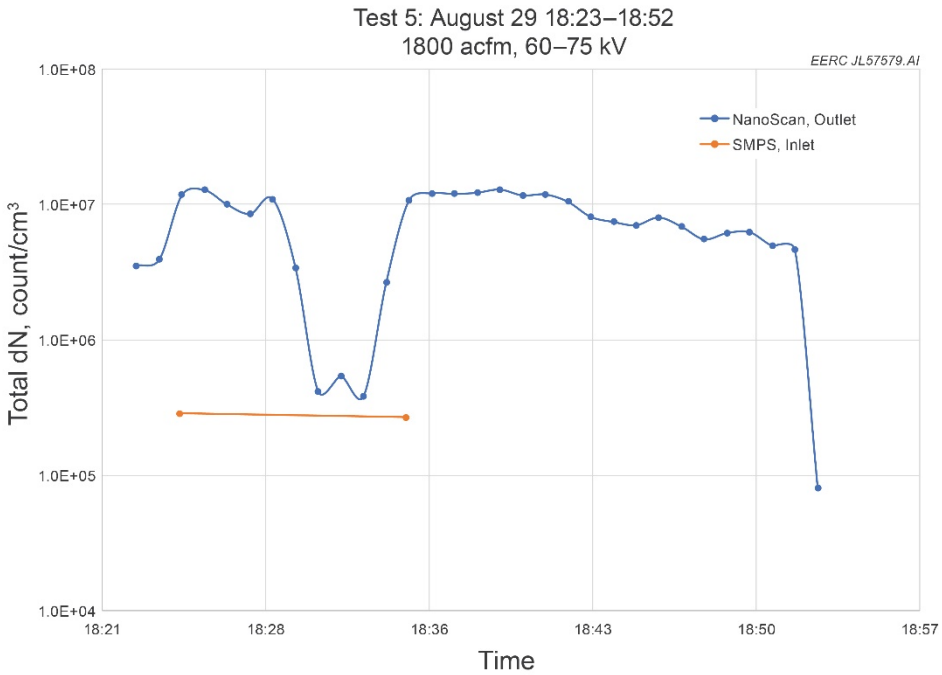

Figure A-13. Test 5 total aerosol concentration.

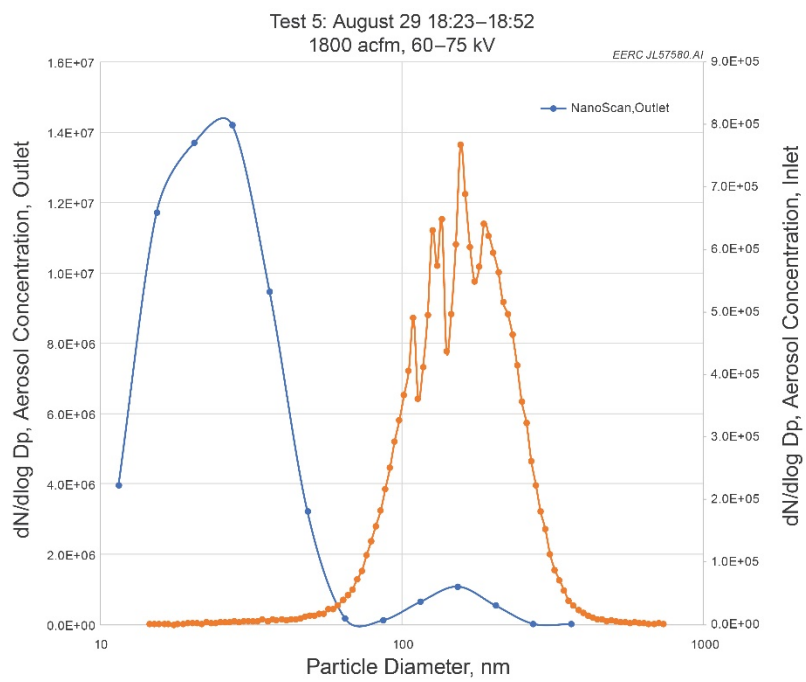

Figure A-14. Test 5 average PSD.

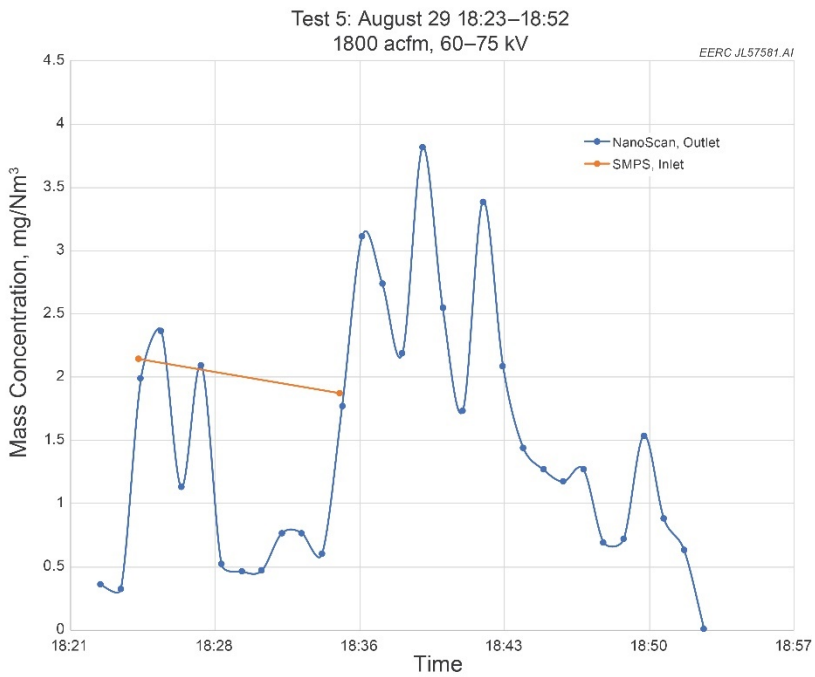

Figure A-15. Test 5 aerosol mass concentration.

TESTS 1–5 COMPARISON

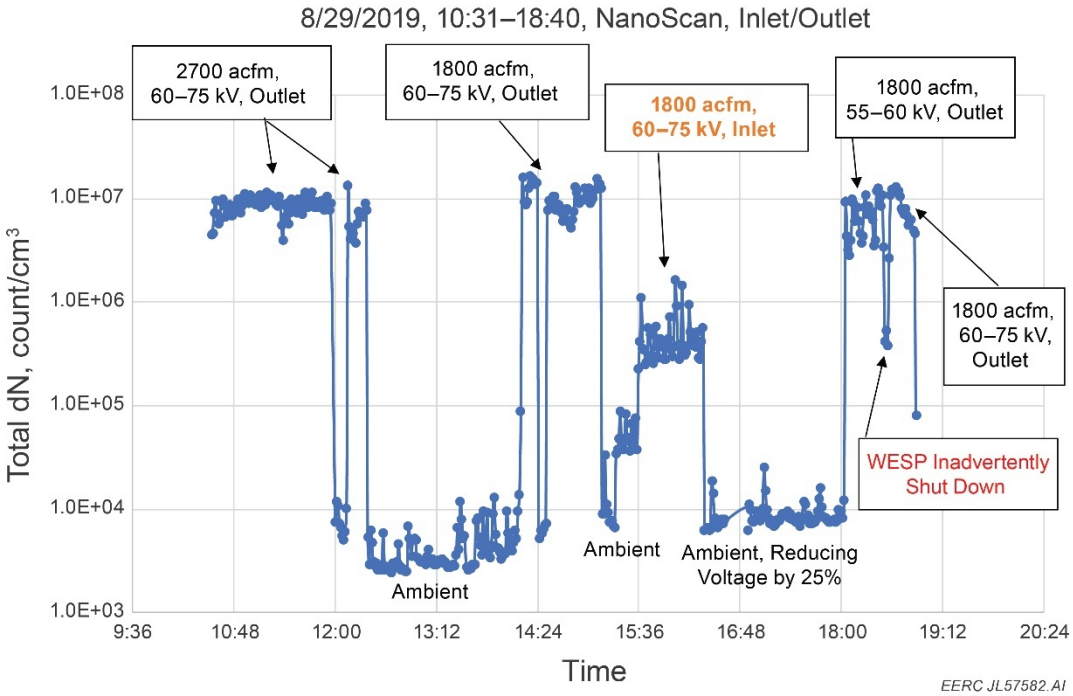

Figure A-16. Total aerosol concentration from NanoScan for Tests 1–5.

TEST 6

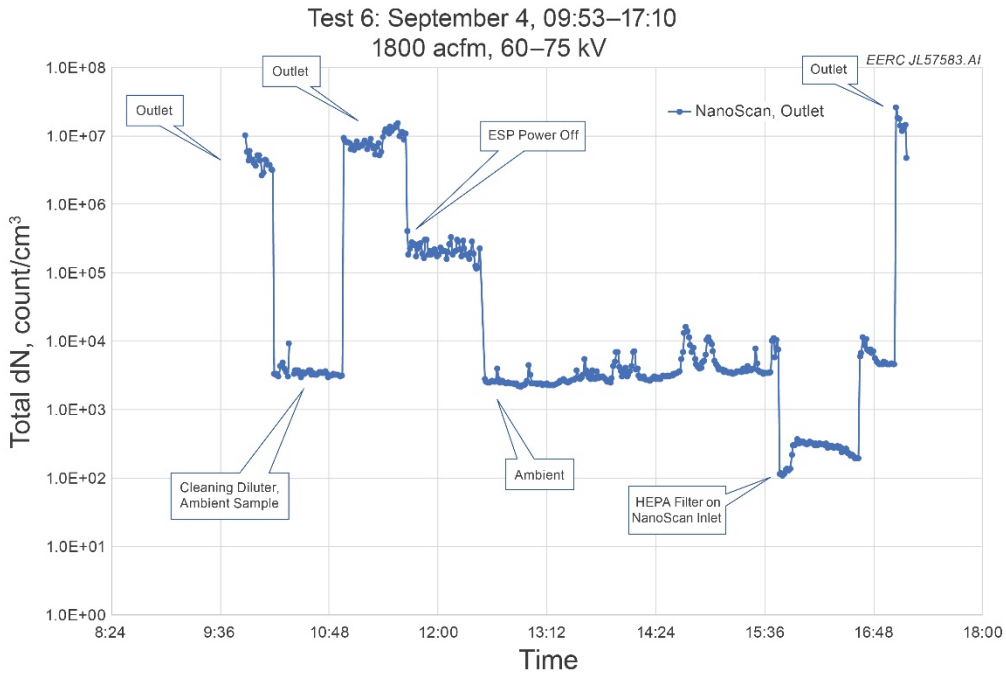

Figure A-17. Test 6 total aerosol concentration.

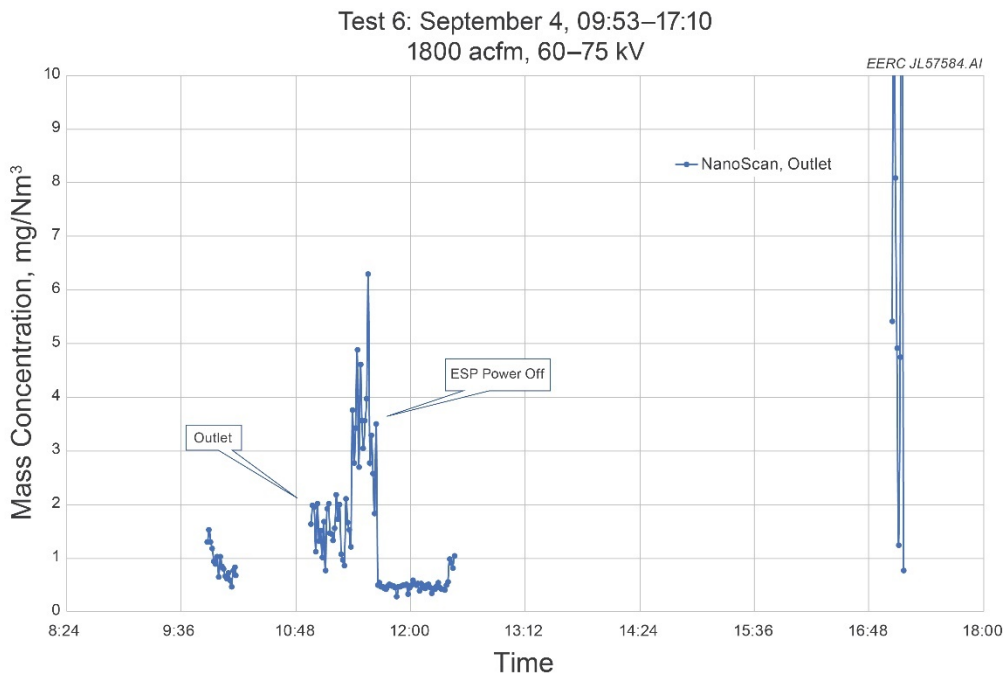

Figure A-18. Test 6 aerosol mass concentration.

TEST 7

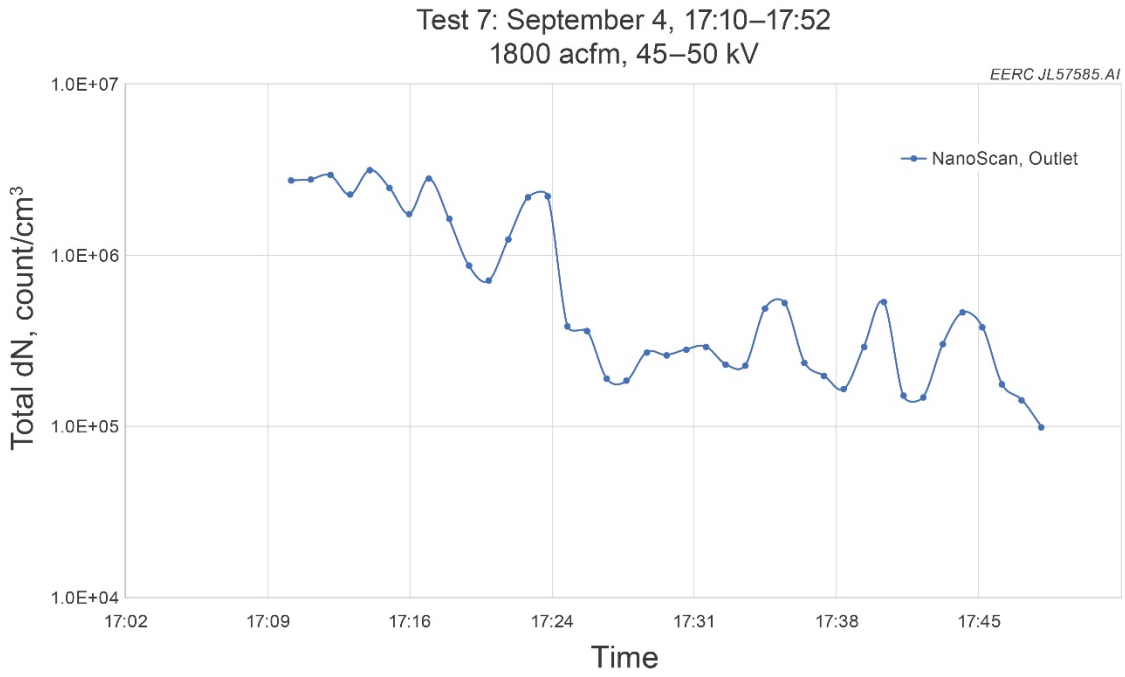

Figure A-19. Test 7 total aerosol concentration.

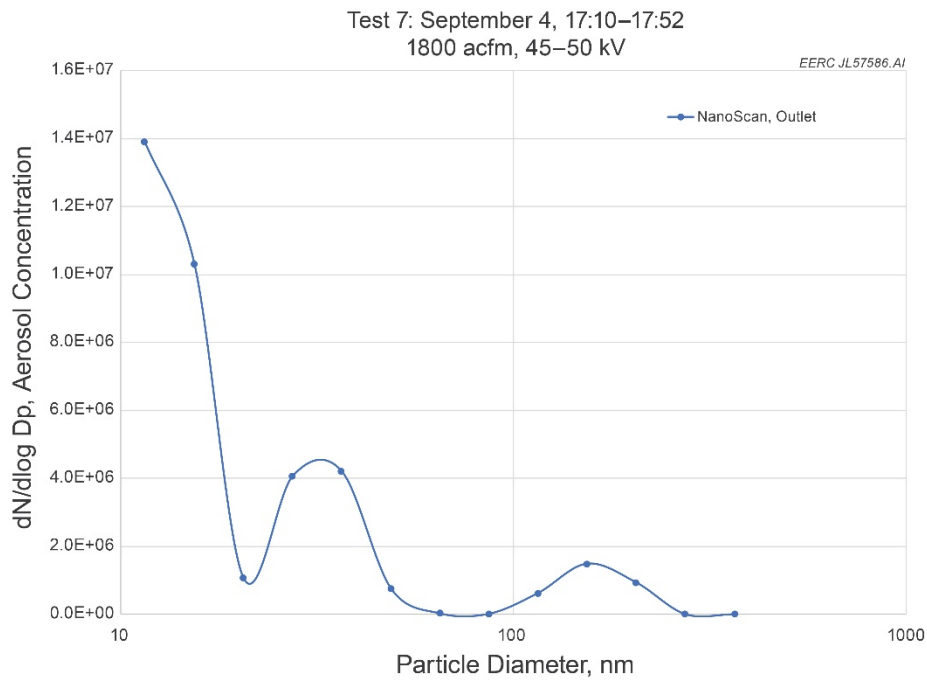

Figure A-20. Test 7 average aerosol PSD.

TEST 8

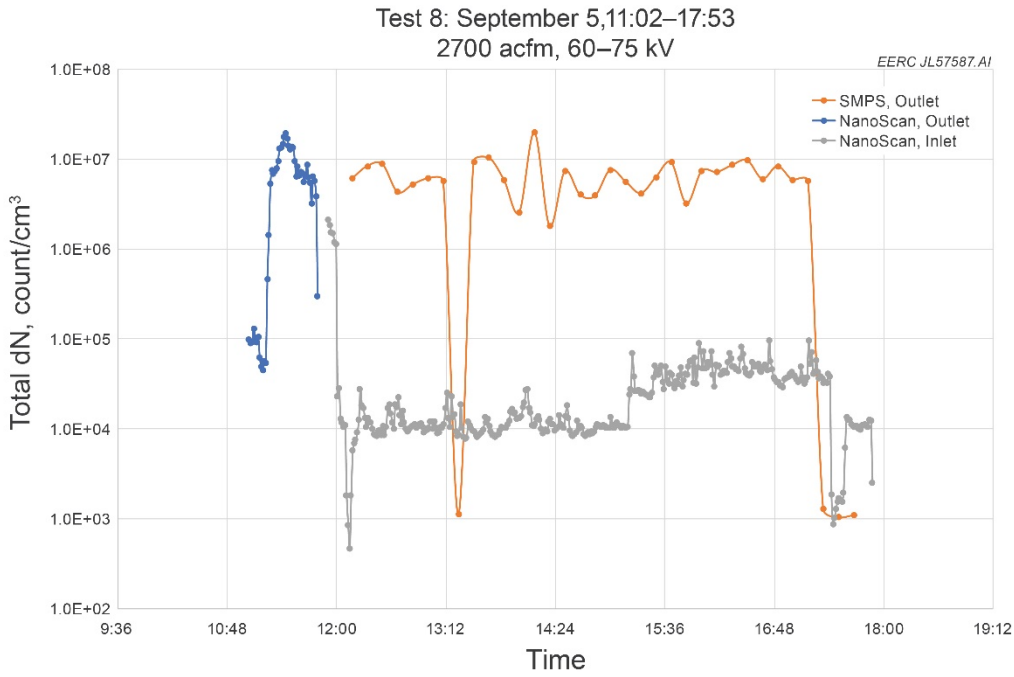

Figure A-21. Test 8 total aerosol concentration.

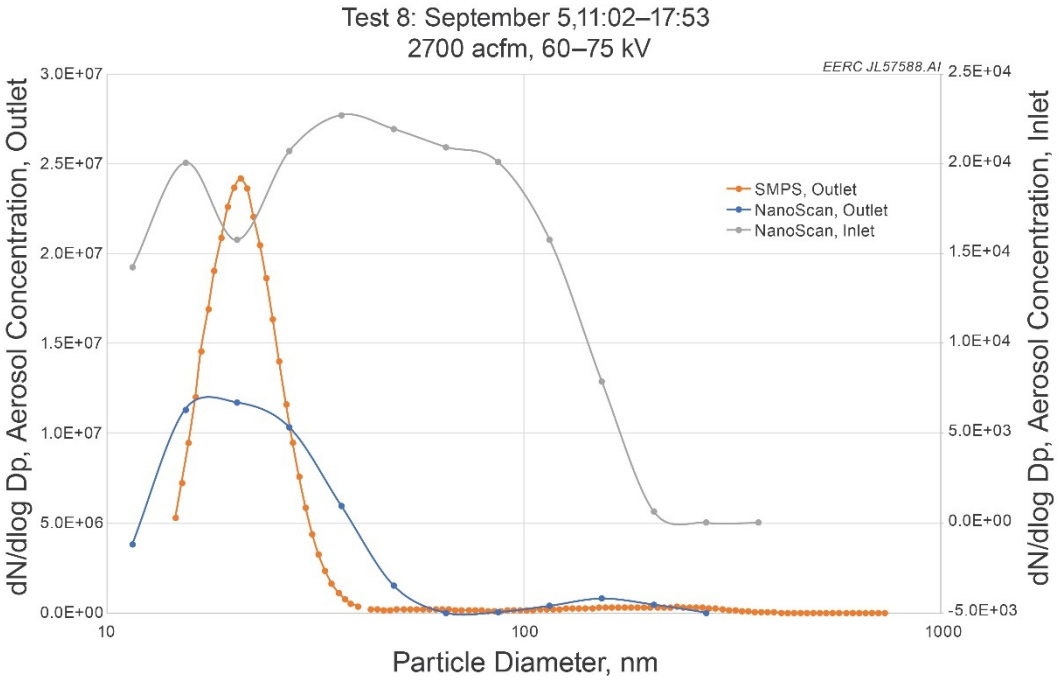

Figure A-22. Test 8 average PSD.

TEST 9

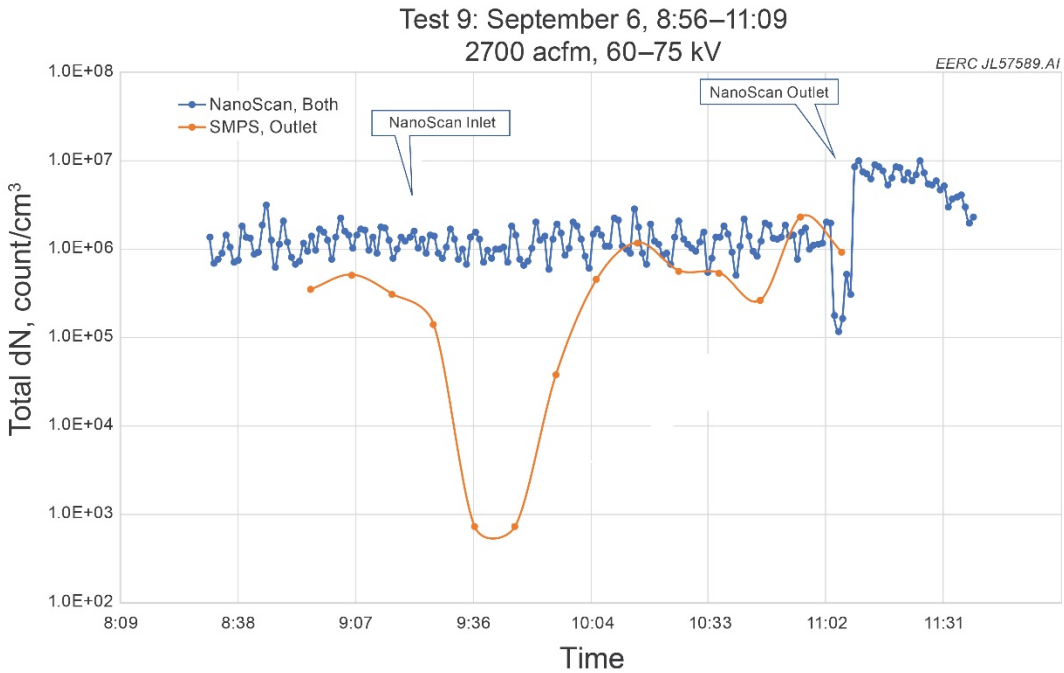

Figure A-23. Test 9 total aerosol concentration.

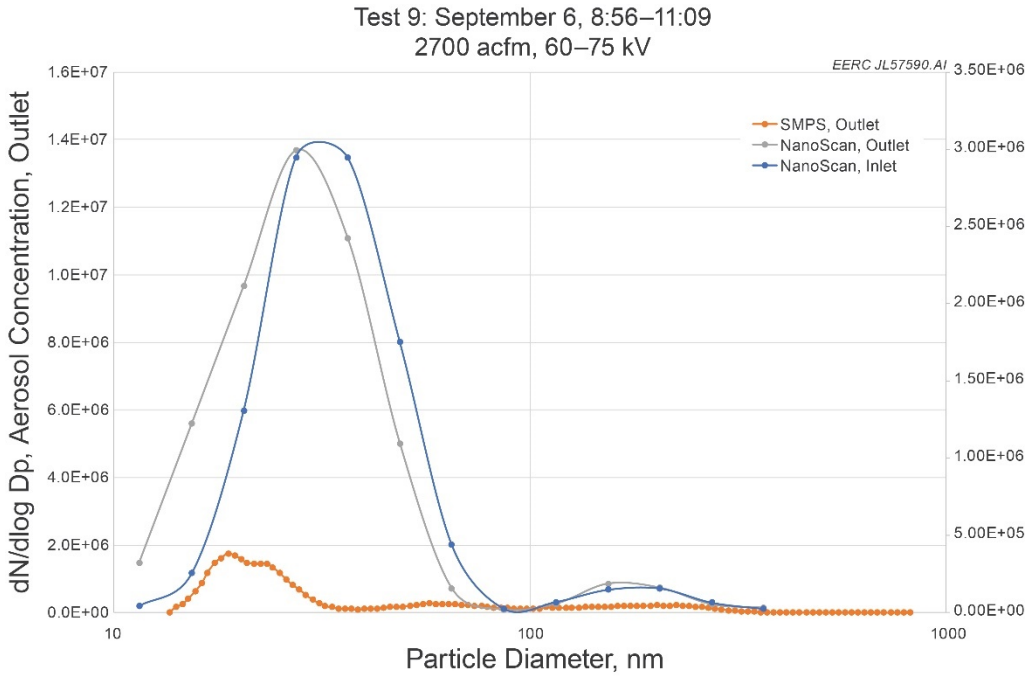

Figure A-24. Test 9 average PSD.

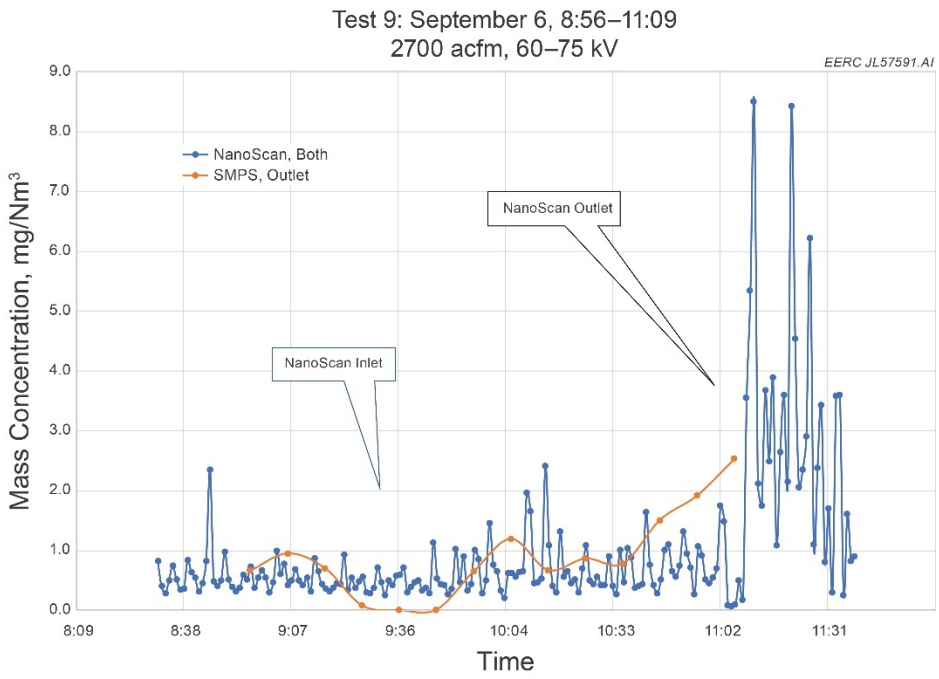

Figure A-25. Test 9 particulate mass concentration.